Tampere University

Lauri Aaltonen

IMPROVING LIGHTNING IMPULSE MEASUREMENT SYSTEM OF TAMPERE UNIVERSITY

Hardware development and uncertainty evaluation

Master of Science thesis
Faculty of Information Technology and Communication Sciences
Examiners: Docent Kari Lahti
D. Sc. (Tech.) Pertti Pakonen
May 2022

ABSTRACT

Lauri Aaltonen: Improving lightning impulse measurement system of Tampere University
Master of Science thesis
Tampere University
Master's Degree Programme in Electrical Engineering
May 2022

Electrical grids' components are tested with standardized lightning impulses to ensure their capability to withstand stresses caused by lightning phenomena to ensure a strong network. Currently the trends in transmission networks are towards higher system and test voltages which generates the need for better calibration capabilities. This thesis focuses on development and characterization of Tampere University's lightning impulse measurement system. The system is studied because it is needed to be prepared for an European intercomparison campaign, where reference level uncertainties are necessary.

The old system was altered by adding a new low voltage arm to the damped capacitive high voltage divider as well as a new measuring cable. Thorough initial characterizations were carried out for the existing measuring system. It was found out that the HV arm's elements exhibit unidealities that result in high oscillations in the divider's response. The high voltage arm's capacitance also exhibits frequency dependency which is compensated in the new low voltage arm by adding a compensation branch to the printed circuit board. Together with simulations and step response testing, analysis of different improvements are carried out in order to improve divider's dynamic performance. The compensation is also tuned with step response tests. The uncertainty contributions are studied with different testing setups or by estimation.

The different standard uncertainties for the voltage divider are examined and uncertainty analysis performed using a reference measurement system method. The peak voltage and time parameter uncertainties are presented and compared for three different measurement systems. Accuracy of the time to half value is successfully improved by the added compensation.

Keywords: voltage divider, uncertainty evaluation, lightning impulse, calibration, high voltage measurement system

TIIVISTELMÄ

Lauri Aaltonen: Tampereen yliopiston salamasyöksyjännitteen mittausjärjestelmän kehitys
Diplomityö
Tampereen yliopisto
Sähkötekniikan DI-ohjelma
Toukokuu 2022

Sähköverkkojen komponentit, kuten muuntajat, testataan standardimuotoisilla salamasyöksyjännitteillä todennuksena siitä, että komponentti toimii suunnitellusti myös esimerkiksi ukonilman aiheuttamien jänniterasituksien aikana. Tämä varmistaa komponentin luotettavan toiminnan verkossa. Tällä hetkellä kehityssuunta sähköverkoissa on nostaa jännitetasoa siirrettävän tehon kasvattamiseksi. Kasvava jännitetaso aiheuttaa kasvavat vaatimukset kalibrointikyvylle. Tämä opinnäytetyö keskittyy Tampereen yliopiston salamasyöksyjännitteen mittausjärjestelmän kehittämiseen ja karakterisointiin. Järjestelmä pitää valmistella eurooppalaista vertailumittausta varten, jossa referenssimittausjärjestelmiltä vaadittavat mittausepävarmuustasot ovat vaatimuksena.

Vanhaa olemassa olevaa järjestelmää kehitettiin suunnittelemalla ja rakentamalla uusi alajänniteosa vaimennettuun kapasitiiviseen jännitteenjakajaan, sekä uusi mittauskaapeli. Järjestelmän jännitteenjakajan yläjänniteosan komponentit osoittivat epäideaalisuuksia, mikä aiheutti järjestelmän vasteeseen suuria värähtelyjä. Yläjänniteosan kapasitanssi oli taajuusriippuvaa, joka on kompensoitu uudessa alajänniteosassa lisäämällä alajänniteosan piirilevyn kondensaattoreiden rinnalle kompensointihaara. Erilaisten parannuskeinojen toimivuutta on analysoitu yhdessä simulointien ja askelvastemittausten avulla. Myös kompensointihaara on mitoitettu askelvastetta käyttäen. Epävarmuustekijät on määritetty erilaisilla testausjärjestelyillä tai arvioimalla.

Kullekin vaihtoehtoiselle mittausjärjestelmälle on laskettu kokonaisepävarmudet standardiepävarmuuksien ja referenssijärjestelmän kanssa suoritettujen vertailumittausten pohjalta. Kolmelle eri mittausjärjestelmälle määritetyt kokonaisepävarmuudet jännitteen huippuarvolle sekä aikaparemetreille on esitetty ja erisysteemejä vertailtu keskenään. Salamasyöksyjännitteen selän puoliarvoajan epävarmuus on parantunut huomattavasti suunnitellun kompensointihaaran avulla.

Avainsanat: jännitteenjakaja, epävarmuusarvio, salamasyöksyjännite, kalibrointi, suurjännitemittausjärjestelmä

PREFACE

This thesis was written for the High Voltage research group of Tampere University in close collaboration with VTT Technical Research Centre of Finland. Firstly I want to thank adjunct professor Kari Lahti for the help and supervision during the completion of my thesis. Also I want to thank research scientist Jussi Havunen and senior scientist Jari Hällström for providing me with useful advice.

Tampere, 18th May 2022

Lauri Aaltonen

This project (19ENG02 FutureEnergy) has received funding from the EMPIR programme co-financed by the Participating States and from the European Union's Horizon 2020 research and innovation programme.

CONTENTS

LIST OF SYMBOLS AND ABBREVIATIONS

AC	Alternating current
DC	Direct current
EURAMET	The European Association of National Metrology Institutes
FutureEnergy	Project name for: "Metrology for future energy transmission"
HVA	High voltage arm of a high voltage divider
LI	Lightning impulse
LVA	Low voltage arm of a high voltage divider
NMI	National Measurement Institute
PCB	Printed circuit board
SG	Spark gap
SI	Swightning impulse
TAU	Tampere Universities
VTT Mikes	VTT Technical Research Centre of Finland: the Centre for Metrology and Accreditation
HV	High voltage
a	number of pulses performed for a single voltage level
b	number of voltage levels used
C	capacitance
c	sensitivity coefficient
f	frequency
T_1	front time of a lightning impulse
L	inductance
η	utilization factor
R	resistance
F	scale factor
τ	time constant for series RC circuit
T_2	time to half-value of a lightning impulse

u_A	type A standard uncertainty
u_B	type B standard uncertainty
U	expanded uncertainty
V	voltage

1. INTRODUCTION

Power grids' equipment need to be tested to ensure security of the power supply for customers as well as to protect the network from blackouts. The voltage stresses on components are generally of two types: the normal operational voltages and overvoltages. The overvoltages can be caused by e.g. a lightning strike, a fault in the network or a switching event. The components are tested with standardised voltages by testing laboratories to ensure their connectability to the network. The overvoltages need special measurement systems to measure the voltage applied to the device under test. Usually the system consists of a recorder instrument, a transmission cable and a voltage divider. The outcome of this thesis is to explain the theory of impulse voltage testing, develop a new measurement system and evaluate uncertainties of different measurement setups.

The thesis was done as a part of an EU-funded project called "Metrology for future energy transmission" abbreviated as FutureEnergy. The project focuses on expanding the traceability of the measurements for higher voltages. One of the project outcomes is to extend lightning impulse measurement traceability to 2.5 MV voltage level for which also the lightning impulse measurement system of Tampere University is developed further. To ensure traceability of the measurements, an intercomparison campaign is held at the end of the project.

The conclusions of the project will help to meet with the future demand for higher voltages used in transmission grids. Improving the uncertainty as well as implementing traceability will allow for more precise safety margins. This will result in loss minimization and improved quality of high voltage systems.

The thesis will explain the theory of impulse voltage generation, definitions for impulse overvoltages, measurement of high impulse voltages, uncertainty components for high voltage measurement systems, development methods to improve the existing system and address the uncertainties of the old and new systems. First, the theory of high voltage impulse measurements is explained. The generation of impulse voltages is addressed first to understand how the impulse voltage is formed in high voltage laboratories and how the impulse voltage gets its shape. Then the measurement systems needed to measure high voltages are explained with emphasis on impulse voltage measurements. After that the measurement uncertainty and standard uncertainties regarding impulse voltage

measurements are introduced.

The empirical part of the thesis will introduce the measurement systems under examination at first. Then the different improvements, that have been carried out mainly on the low voltage arm, are explained. Finally the uncertainties for the systems are evaluated and compared against each other and the requirements for a reference system.

2. THEORY OF HIGH VOLTAGE IMPULSE TESTING

Electrical grid and its connected equipments' insulators are designed to withstand normal operational voltages caused by load and generation variations in the grid as time passes. Different overvoltages can cause additional stresses to the insulators. Transient overvoltages can occur during switching, fault or direct or indirect lightning strokes. Therefore insulators in the grid or in grid connected apparatus should be designed to withstand also these faster transient over-voltages. [1, p. 253][2, p. 285]

In addition to component withstand against the over-voltage impulses, sometimes the breakdown mechanisms that occur in the test object during transient overvoltages are studied [3]. If the component doesn't tolerate the voltage applied, a puncture or a flashover occurs which causes the applied voltage to collapse.

Lightning (LI) and switching impulses (SI) are characterized by the peak voltage value and the time parameters of the pulse i.e. the shape of the pulse. That has also a large impact on how the insulator will tolerate the voltage. [1]

2.1 High voltage impulses

Impulse overvoltages are unidirectional voltages that rise quickly from zero to the peak value and then more slowly down back to the zero. The impulse waveforms always have some oscillations and therefore IEC-60060:1 standard defines LI pulse as being a transient voltage, which usually rises rapidly to peak value and then more slowly to zero [4, p. 26]. The word "usually" applies to more general LI wave shapes, there still being room for some exceptions like chopped LI waves. The standard has stated only one numerical value that defines an impulse voltage to be specifically a lightning impulse voltage and that is the front time T_1 being less than 20 µs [4, p. 26]. A typical standard lightning impulse voltage is shown in figure 2.1.

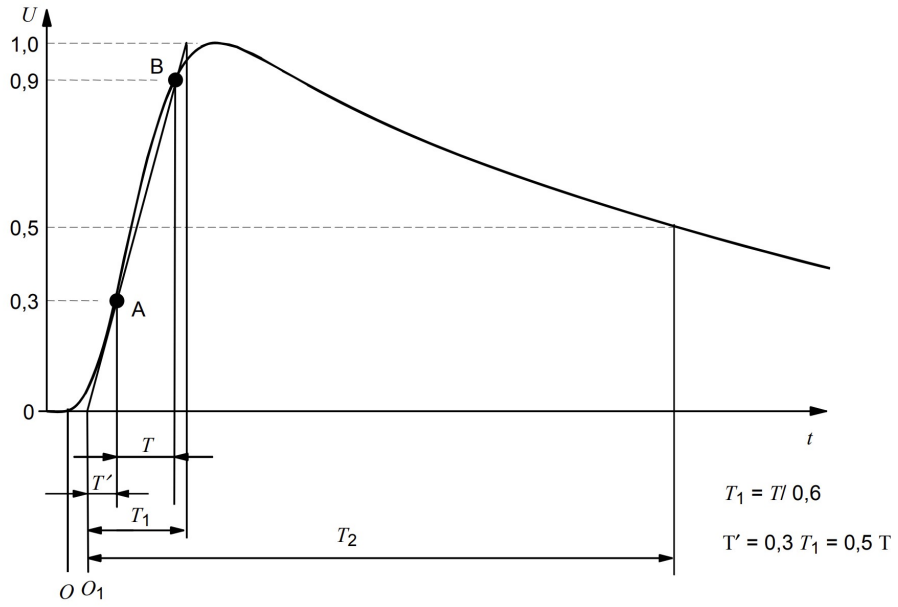

Figure 2.1. *Full LI with time parameters [4].*

The parameters of a LI impulse are complex to determine. The standard shape used in lightning impulse tests is 1.2/50 meaning the front time being 1.2 μs ± 30 % and time to half value being 50 μs ± 20 % and the test voltage's maximum value itself being around ± 3 % [4].

The values are complex to determine, especially the peak value. The standard [4] states that after base level offset is corrected, the measured data should be used to make a double exponential fit-curve. Now this double exponential substracted from the zero level corrected curve, which gives the oscillations present in the LI test voltage. Oscillations are caused by inductances being present at the measurement system that cannot be fully avoided [5]. Now the curve with just the oscillations is multiplied with a specific test voltage curve that is basically a low-pass filter. Then that filtered oscillation curve is added back to the double exponential. The peak value is to be taken from this resulting curve but the time parameters should be taken from the double exponential curve. [1] This is because the resulting curve with damped oscillations on top of the ideal double exponential –also called by a term base curve– is the worst case considering the stresses in insulating material but if those oscillations are kept there, especially the front time would be sensitive to the oscillations.

When the final curves are obtained, the parameters are taken. The front time T_1 is taken by drawing a straight line between 30 % and 90 % points of the curve and then measuring that straight line's rise time from 0 to 1 normalized amplitude. The time to half value T_2 parameter is taken from the time difference of previous mentioned straight line's intersection with x-axis and the time the curve reaches halfway point in the tail of the impulse. [4]

The general LI waveshape can also be chopped. The chopping is done via a chopping gap and the chopping can be done during the front, the peak or the tail of the impulse. The standard time to chopping is between 2 to 5 µs. The chopping can be done during the front of the impulse or during the tail. The chopping shall be steeper compared to the rise of the LI. [6] Figure 2.2 shows an example of a chopped pulse.

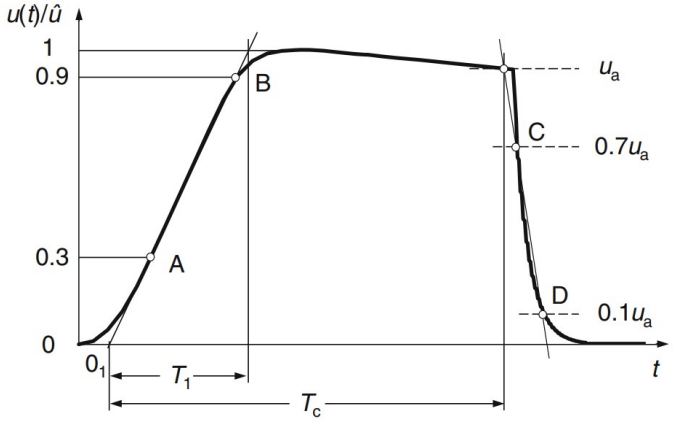

Figure 2.2. *Chopped LI with time parameters [6]*

The worst case for the insulating material is when the chopping is done near the peak due to the fast voltage collapse. Tests with chopping simulate the operation of protection devices in the network like surge arresters or the effect of a breakdown in the HV circuit. [2]

Switching impulses SI are similar to lightning impulses. Both are double exponential aperiodic impulses but the main difference is that switching impulse has significantly larger time parameters, the standard shape being 250/2500 µs. The IEC standard distinguishes between SI and LI by defining SI by having a front time of 20 µs or more. [4] The peak parameter is taken from the maximum voltage recorded. The time to peak value is taken from the true origin and the time when peak voltage value is reached. The time to half value is taken from the true origin to the time when half of the peak value is reached at the impulse's tail. Noticeable difference is that SI evaluation doesn't use filtering or virtual origin as LI does. [6] The slower SI has less unwanted oscillations appearing in the waveform caused by inductance in the circuitry and nonuniform spark gap operation so there is also less need to do additional filtering of the signal.

2.2 Generation of impulse voltages

Figure 2.3 shows a basic one stage circuit block used to generate LI and SI over-voltages. First, the input capacitor also called charging capacitor is charged through high resistance valued charging resistor. Then the switch –a controllable spark gap called trigatron [1]– is closed or closes itself if the breakdown voltage is achieved. Now the impulse voltage

is formed by charging the load capacitor through front resistor that forms the front of the impulse voltage and at the same time the impulse capacitor is discharged through tail resistor that defines the tail of the impulse voltage. [2, 3]

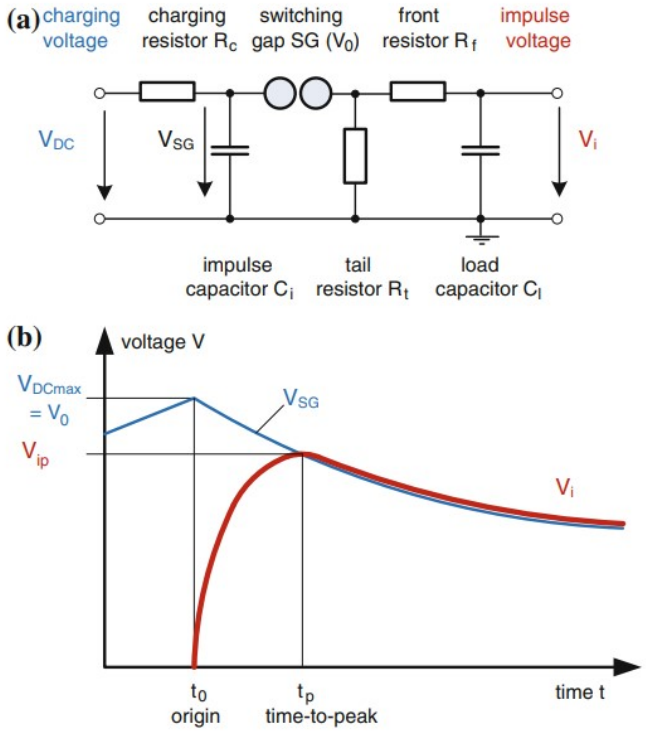

Figure 2.3. *Impulse voltage forming circuit and potential diagram [2].*

The time parameters of the impulse are mostly based on the RC time constants in the circuit shown in figure 2.3. When the spark gap ignites at t = 0, almost immediately the full charging voltage applied to impulse capacitor appears at the series combination of R_f and C_l. The faster time constant the combination has, the faster the voltage rises to the peak value across the capacitor C_i. [2, 3]

The peak voltage achieved cannot be greater than the charging voltage available in the charging capacitor. Utilization factor

$$\eta = \frac{V_{i,max}}{V_0} \approx \frac{C_i}{C_i + C_l}, \tag{2.1}$$

where $V_{i,max}$[1] is the maximum value of the impulse voltage, V_0 is the breakdown voltage of the switching gap, C_i is the impulse capacitor and C_l is the load capacitor. The utilization factor should be as close to 1 as possible so i.e. choosing $C_i >> C_l$. This can't be achieved since some energy converts to heat in the resistors and the capacitor's difference in values isn't extremely high. [1, 2]

[1] symbol "V" is used for voltage since uncertainty often is denoted by a symbol "U"

This single-stage circuit will work up to a relatively low voltage level. When increasing the voltage level, difficulties arise due to the physical size of the circuit elements, spark gap operation, the much higher DC voltage needed and the increased need for shielding to suppress corona discharges. [5] The solution to overcome this is to add multiple single-stage circuits –shown in figure 2.4– so that the capacitors will charge in parallel and discharge in series. [2, 7]

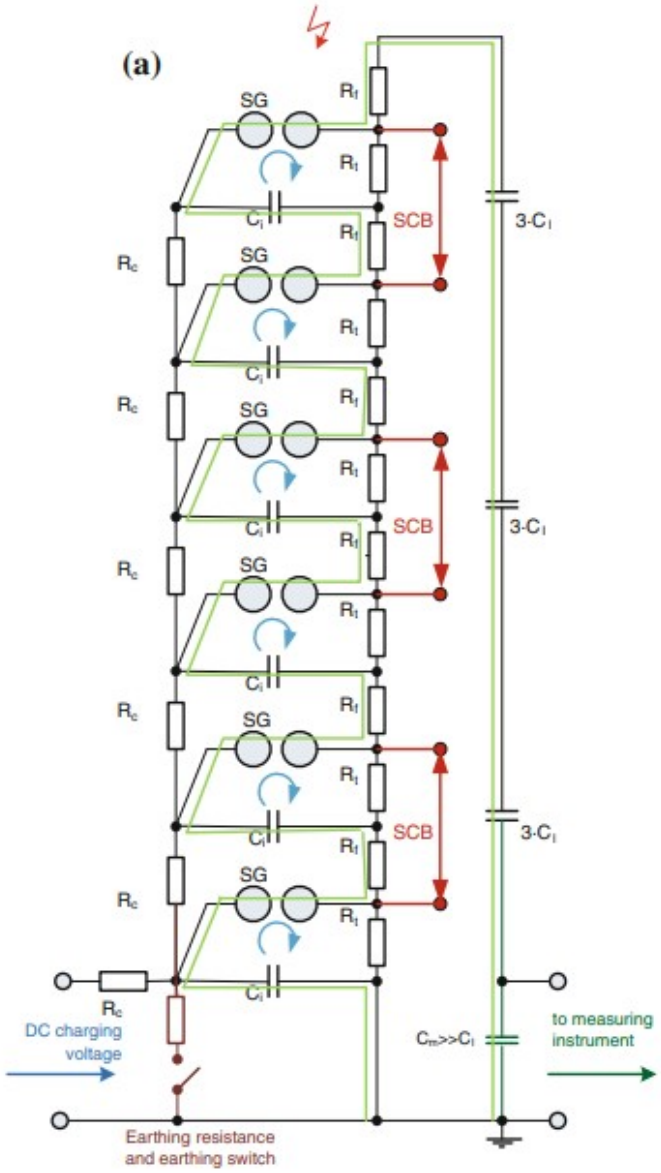

Figure 2.4. *Impulse voltage forming Marx circuit [2].*

The parameters of the impulse are formed from the Marx generator's capacitances and resistances, the impedance of the device under testing and the whole testing circuit's inductances [7]. All the stages of the generator are charged equally with a constant current until all the stages are at a desired voltage. Then the switching gap is triggered at the lowest stage.

The triggering is done with a trigatron, a small device, that causes small discharge at the lowest gap. This breakdown voltage is the lowest trigger limit of the generator. If the trigger voltage is too high, a self-discharge is generated. The trigger voltage of the trigatron therefore has 2 limiting factors.

When trigatron is triggered, the switching gap at the lowest generator stage is trigged causing the overvoltage appear on the second stage. From there the overvoltage trips the second switching gap and consecutively travels to the top of the generator as a travelling wave. [2]

2.3 Measurement of high impulse voltages

The measurement system of high voltages consists normally of large elements. This results in special compromises regarding measurement quantities such as time and voltage values. Measurement system is connected to the device under test so it will affect to the measured waveforms. Also the connectors and other elements are open structures so there are significant stray elements affecting the measurements.

The measuring device can be a sphere gap if the only interesting value is the peak voltage. Measuring the peak voltage by this method also needs artificial irradiation for example an UV light to reduce the scatter of the breakdown delay in case of low LI voltages [3]. Nowadays the sphere gaps are used mostly in routine checks and linearity tests. Voltage dividers are used when the whole waveform and its parameters are needed. Voltage divider setup consists of a converting device –a voltage divider– and a measuring instrument –such as an oscilloscope– and a transmission system that is usually a coaxial cable. [2]

The system shown in figure 2.5 consists of an impulse generator, a device under test, a damping resistor, connector leads and cables, a voltage divider and measurement device. The measurement devices such as an oscilloscope has their own standards and the other parts of the measurement system –in the case of impulse voltages– has IEC-60060 standard.

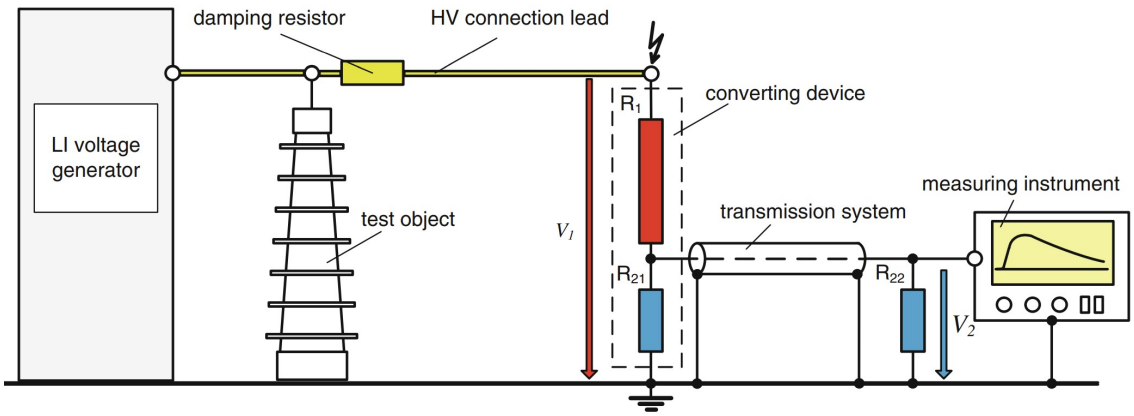

Figure 2.5. *Complete LI testing system. [2]*

Measurement system has a so called scale factor that indicates the attenuation amount of the converting device. The measured high voltage is attenuated by the converting device such as a voltage divider to be more suitable for the oscilloscope. The real voltage on the test object's terminals can be calculated from the recorded, attenuated, waveform by multiplicating it with the scale factor. The system also has dynamic characteristics that should be designed according to the timescale needed for the measurements. [1]

2.3.1 Voltage dividers

LI voltages are mainly measured with a voltage divider and an oscilloscope or a digitizer. A voltage divider is a series connection of two different valued impedances. The dividers can be resistive, capacitive, damped capacitive or a combination of these. Different types of dividers have different applications. [1]

An ideal divider should be designed in such a way that both the low voltage and high voltage arms have same time constants. This means that

$$\frac{R_1}{R_2} = \frac{L_1}{L_2} = \frac{C_1}{C_2}, \tag{2.2}$$

where R, C and L are the parameters of the divider shown in figure 2.6. When equation 2.2 is met, the RC and LC time constants are equal and when feeding an ideal square wave to the input, an ideal square wave is produced at the output but scaled to a lower voltage. [8]

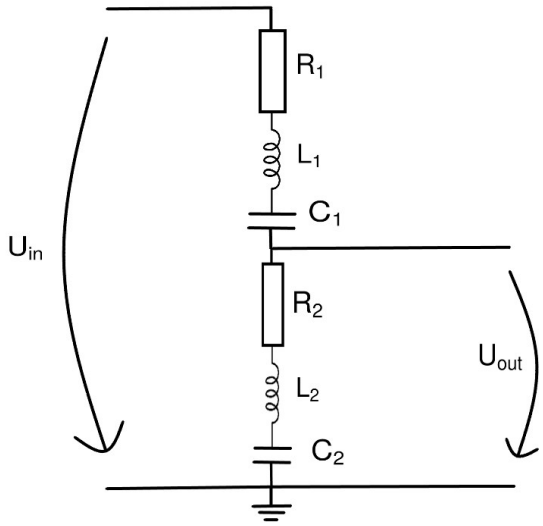

Figure 2.6. *Equivalent circuit of a general divider.*

In reality the equation 2.2 conditions are never fully met. There are stray elements between different points such as stray capacitance from the top of the divider to the low voltage arm, different temperature dependencies of the elements and other unidealities. This will affect the transfer function of the divider and for example make the output more oscillatory or slower than ideally.

There are many different types of voltage dividers. In a case of high voltages, the most relevant divider types are shown in figure 2.7.

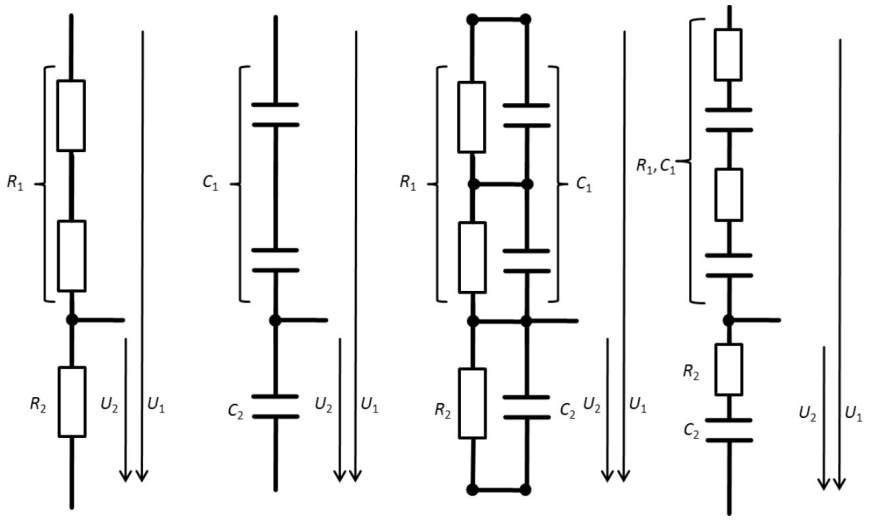

Figure 2.7. *Divider circuits. [9]*

The first divider is a resistive divider. Resistive dividers are mostly suitable for DC and impulse voltages [9]. The second, capacitive, divider is best suitable for AC measurements and is unsuitable for DC measurements since DC current cant flow through a capacitor.

The third divider in figure 2.7 is a capacitive-resistive divider or so called universal-divider that has a parallel resistive and parallel capacitive branches to be able to capture as well DC but also AC voltages. The last divider is called a damped capacitive or a Zaengl divider. It is a capacitive divider with added damping resistor to HVA and LVA. This type of a divider is mostly used in LI and SI measurements. Whereas resistive divider is only applicable for for SI or LI depending on its construction the damped capacitive divider has capacitance to measure the fast transient in the front of the impulse as well as measuring the slower decaying tail. The damping resistor is used to reduce the oscillatory behavior of a fully capacitive divider. [10]

The dividers generally, when the voltage levels increase to several hundred of kilovolts, have an open structure. This means that especially when considering fast transient phenomena like a lightning impulse, the parasitic elements start to play a big role. The stray capacitance to ground and other nearby objects and inductances f.ex. in the damping resistors are noticeable at high frequencies. The relevant stray capacitances are shown in figure 2.8.

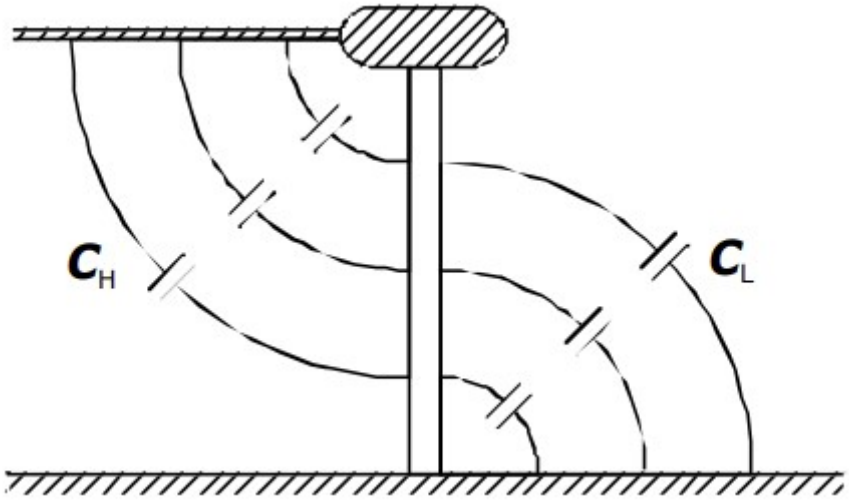

Figure 2.8. *Divider stray capacitances. [8]*

In the figure 2.8 C_H is the capacitance from some point in the divider to the energized object, in the picture the connecting lead that is usually a copper strip or an aluminium or copper pipe. The C_E is the capacitance from divider column to ground. These stray capacitances affect the division ratio. [11]

The total earth capacitance of the divider column

$$C_E = \frac{2\pi\epsilon_0 h}{\ln\left(\frac{h}{r\sqrt{3}}\right)}, \tag{2.3}$$

where r is the radius of the divider column and h is the height of the column. This

equation is only applicable when divider is placed near the ground surface. To do more precise calculations, the earth capacitance should be divided along the column so that the capacitance value is highest in the lowest part of the divider. The earth capacitance impacts the division ratio as well as dynamic performance for capacitive and damped capacitive constructions but for purely resistive dividers only the dynamic performance is impacted. [1]

Resistive divider

Resistive dividers are used in measuring high transient voltages in the µs range. Regarding less fast transients such as switching impulse voltages, this type becomes less eligible due to too high divider loading [6]. Resistive divider's dynamic performance which affects the uncertainties is mainly affected by stray capacitances from divider column to earth. The resistive part with the stray capacitance to ground will form an RC low pass filter and thus making the resistive divider unsuitable for measuring fast transients. If the electric field is linearized along the column via extra electrodes or the if the high voltage resistor is wound to match the field, then the resistive divider can be used to capture high transients. Going into higher voltages, the size of the shielding rings will get bigger which produces more stresses mechanically and thus limit the voltage range the resistive divider can be used in. [2, 8]

The resistance value of the high voltage arm is chosen by the application the divider is in. The higher the resistance is, the lower loading the divider experiences while having slower response and vice versa for lower resistance values [8].

There are 2 types of stray capacitances affecting the transfer function of the resistive divider. The individual resistors in high voltage column have a parallel capacitance and also the stray capacitances from divider column to earth. [11] The equivalent circuit of a resistive divider with stray capacitances lumped together is shown in fig. 2.9.

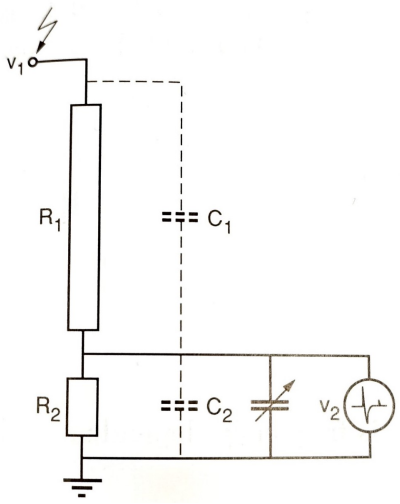

Figure 2.9. *Resistive divider with equivalent parasitic capacitances. [11]*

Now the resistive divider is not ideal anymore so the scale factor also has terms with capacitances. The scale factor

$$\frac{V_2}{V_1} = \frac{\frac{R_2}{1+j\omega R_2 C_2}}{\frac{R_1}{1+j\omega R_1 C_1} + \frac{R_2}{1+j\omega R_2 C_2}}, \tag{2.4}$$

where R and C are the resistances and capacitances shown in fig. 2.9. Now the divider has an RC time constant in the upper and lower part that should be matched similarly to equation 2.2. This can be done by setting up a capacitor in the low voltage with

$$C_2 = \frac{R_1}{R_2} C_1. \tag{2.5}$$

The C_1 is hard to measure so Kreuger [11] suggests that the tuning of the low voltage arm's capacitor should be done by measuring a square wave fed to the divider. The idea is to adjust the capacitor until the measured step response is completely flat. [11]

If the capacitance C_2 is chosen so that it is too small, i.e.equation 2.2 isn't met, the step response of the divider is similar to figure 2.10.

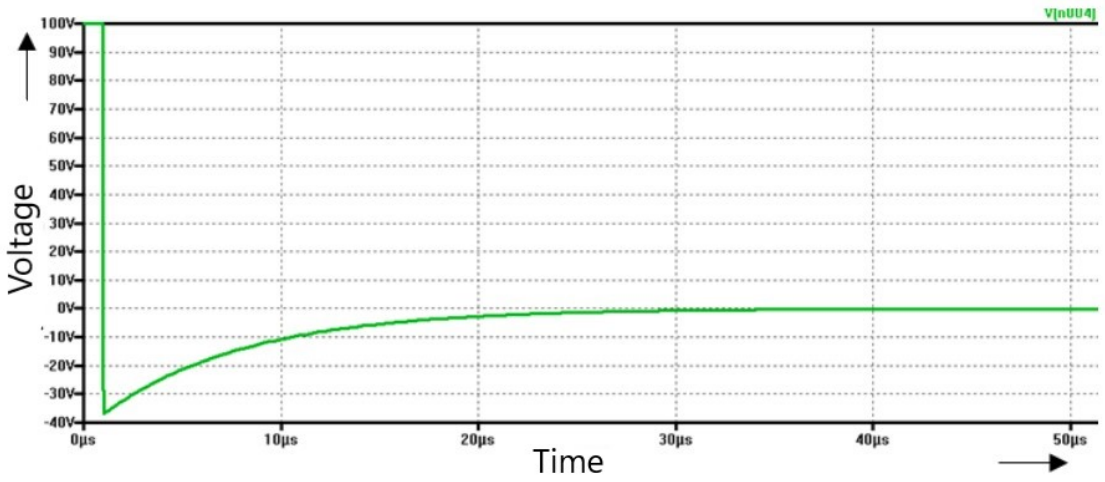

Figure 2.10. *Resistive divider's step response when C_2 is tuned too low. [9, edited]*

If the capacitance is chosen too large, similar phenomena occurs, but in other direction. Now the initial step has undershoot and an increasing trend towards the unit level. [9]

2.3.2 Damped capacitive divider

Damped capacitive divider is used when resistive divider would lower the LI generator's output voltage and duration of the pulse too much and possibly also heat up the divider. Also resistive dividers need field grading rings that increase in size when increasing voltage level. So the resistive divider is suitable for LI and SI only in the lower voltage levels since the mechanical stability concerns arise. [11]

The damped capacitive divider acts as a resistive divider for high frequencies and as a capacitive divider for lower end of the frequency spectrum. The RC time constant is matched in both the upper and lower parts of the divider.

Damping resistor

Damping resistor is inserted to reduce oscillations in the capacitive divider. The oscillations are demonstrated in figure 2.11 and they are caused by the inductances and capacitances presented in fig. 2.12. The damping resistance is usually divided along the HV divider column while one part being at the top of the divider column. Also when adding resistance to the HV side, also the LV side needs resistance added there, according to equation 2.2.

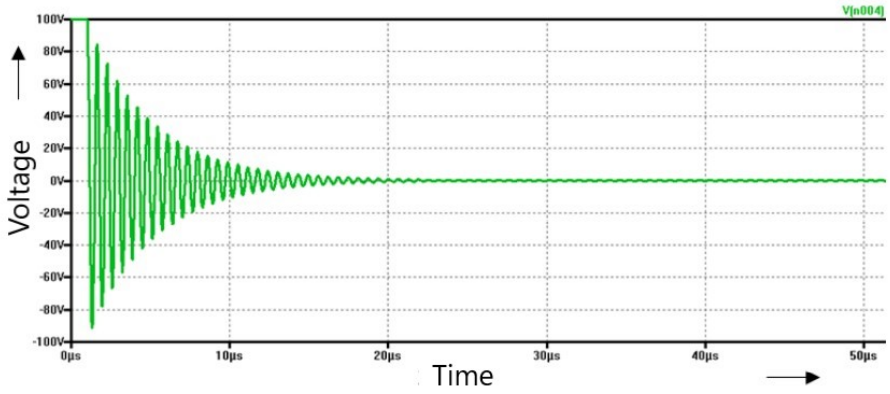

Figure 2.11. *Oscillatory step response of a capacitive divider. [9, edited]*

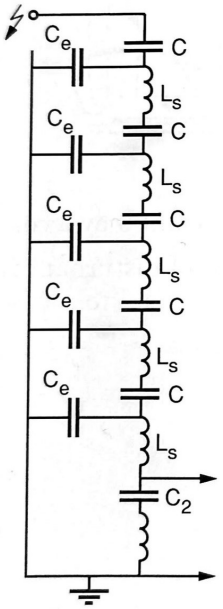

Figure 2.12. *Equivalent circuit of a capacitive divider including the stray elements. [11]*

The inductance of the resistor element is the main concern when it comes to high voltage resistors especially those used in measurement applications. Linearity and stability requirements for the damping resistor can be achieved with proper selection of materials. Usually multiple layers of wire is used to increase the mass of the resistor especially when the damping resistor is used with resistive divider and the component heats up more. The length of the resistor should also be long enough to prevent any flash-overs.

The low inductance is achieved by bifilar winding of the resistance. Bifilarity means that two pieces, or just one in the case for Wenner-type windings, of wire with the same length, are wound on to a core with different direction. The idea is that there is equal number of turns for each wire so the magnetic fields of the two wires cancel each other out. There are different winding formations like Wenner- and Ayton-Perry–windings and also different layering options like a one introduced by McNally [12]. A study by Campisi et al. states

that a Wenner-type bifilar winding arrangement is the most suitable for HV reference divider, out of the winding arrangements tested. Wenner-winding has a additional core that is used to change the winding direction and only one strand of a wire is used. [13] The Wenner-winding idea is demonstrated in figure 2.13.

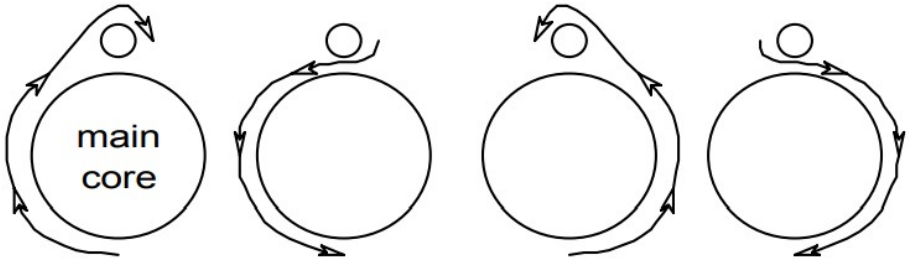

Figure 2.13. *Wenner-winding cross-section. [13]*

The damping resistance should be designed so that the oscillations are damped but not overdamped. The HV resistance should be optimally

$$R = k\sqrt{\frac{L_S}{C_E}}, \tag{2.6}$$

where L_S and C_E are the stray inductance and stray capacitance of the column also shown in figure 2.12 and k is a parameter varying between 2 and 4 depending on literature. [3, 9, 11] The optimal resistance might be bit lower since monotonic step response isn't wanted but a slightly more oscillatory response that has faster rise time, provided that those oscillations occur for only during enough short time interval [6].

Ideally, the damping resistor should be divided inside the high voltage arm, between the capacitors. One large enough part should be left at the top. This is because, when measuring the step response, the resistance at the top could be moved more near the step voltage generator to reduce stray-capacitive coupling effect between the generator and the divider. Also the distribution of the resistance inside the HVA column reduces the stray capacitance effect from the intermediate parts of the divider to ground. If the resistance is only placed at the top, ringing will occur caused by the inductance and capacitance of the circuit.

2.3.3 Capacitive divider

Capacitive dividers are mostly used in measuring of AC and SI voltages. LI voltages cannot be measured with purely capacitive divider because of the oscillatory behavior described in section 2.3.2. The oscillatory behavior is due to the stray inductances and capacitances as well as the travelling wave reflections. [6]

Other disadvantage of the capacitive divider is the exponential decay of the response.

This is caused by the RC-constant in the system. However this can be corrected via a correct selection of a capacitance and a resistance in the divider.

Capacitive divider usually has low capacitance in the HV side so the capacitance of the measurement cable plays a large role on the characteristics of the whole measurement system. The main advantage is that the low capacitance of the whole divider draws very little current and therefore impact on the measured waveform is very small. [14]

2.3.4 Dynamic analysis of voltage dividers

LI voltages have a rise time of approximately 1 µs or even less so the voltage divider should be able to measure those correctly. To be sure the scale factor is stable at even the highest frequencies, the dynamic responce of the divider should be investigated. This is done usually by applying a voltage step of some hundred volts to the divider. The switching action is performed via a mercury-wetted reed relay to gain as steep and ideal voltage step as possible. [2] Other method would be measuring many impulses while varying the time parameters [6].

The dynamic behaviour is determined by the elements itself in the divider but also stray elements the system has like stray capacitances to ground and stray inductance of the damping resistor. The step voltage test can be used in designing the divider's parameters like adding compensation to the LVA to balance unidealities in the HVA that cause a non-ideal step response. Also the step response test can be used to approximate the dynamic behaviour of the divider when calculating the uncertainty of the system.

2.3.5 Damped capacitive divider construction

The high voltage arm consists of many stages of capacitors stacked. The capacitors need to have low inductance. Every stage is housed in insulating housing and oil.

The damping resistance should be divided inside or between the stages of the high voltage arm. One part of the divided damping resistor can be left at the top of the divider or the complete damping resistance can be divided inside the individual stages. The resistor at the top should be wound bifilarly to have a low inductance. The resistors inside the stages should be of a carbon film type. The key points in selecting the resistors are the low inductance, low temperature and low voltage dependancy. Usually the resistors are aged with heat treatment. [11]

The low voltage arm of the divider is connected at the foot of the voltage divider. Carbon film resistors and film capacitors are suitable as the components since they have low self inductance and good impulse voltage withstandability. The resistor–capacitor series connection is usually arranged coaxially in many sections as shown in figure 2.14. This

helps as now the current travelling through the resistors is divided and the self inductance is kept low. [6]

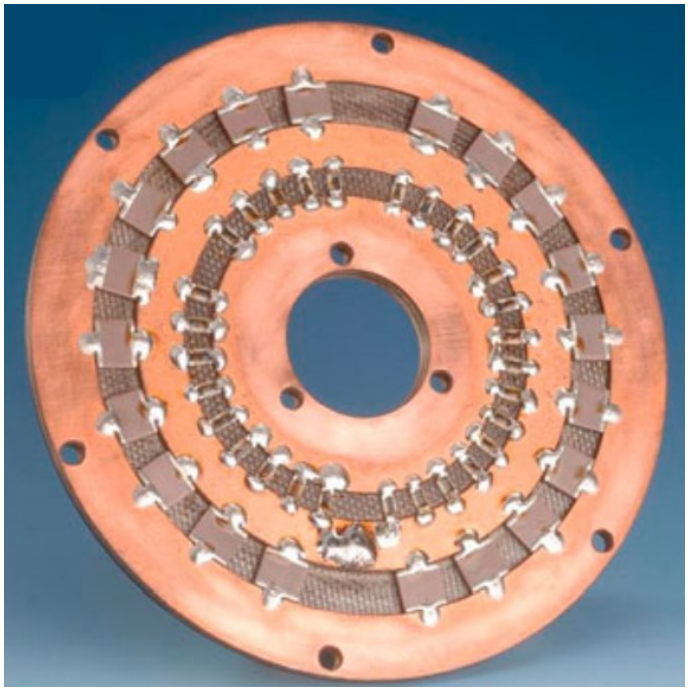

Figure 2.14. *Low voltage arm design on a printed circuit board with chip components. [6]*

The board's middle part is connected to the high voltage arm. The matching resistor, if connected to the LVA and not the recording instrument's end, is placed in the middle of the circuit board and the other end is connected to the connector that the measurement cable is connected. The entire LVA is placed inside plastic or metal housing. [6] In a case of metal housing that is connected to the ground, the connection to the lowest stage of the HVA should have some insulation between the HVA and the LVA part's housing and a feed through connection.

2.4 Frequency dependency of high voltage capacitors

The high voltage divider consisting of multiple high-voltage capacitors may exhibit some non-idealities such as insulating material having some resistance in parallel to the capacitance and also stray capacitances. Li and Rungis discussed in their paper that a damped capacitive divider may exhibit some "creeping" characteristics in the step response due the change of permittivity as a function of frequency in the dielectric material i.e. the high voltage capacitors having some frequency dependency in the capacitor value. An equivalent circuit model of this phenomena is presented in figure 2.15. [15] This characteristic usually has a time span of some tens of μs and therefore affects the uncertainty of the LI waveform's time to half value. This phenomenon has some impact on the front time parameter but that is much smaller in comparison.

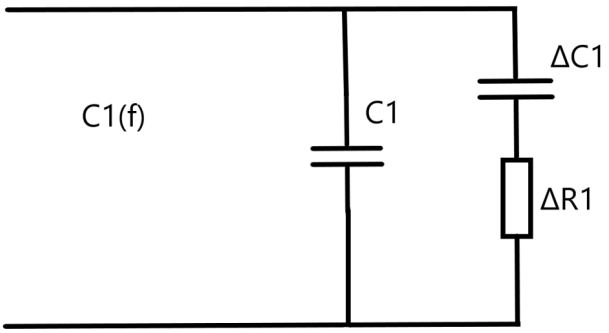

Figure 2.15. *Equivalent circuit model of a frequency dependant high-voltage capacitor. [15, edited]*

In the model, C_1 denotes the asymptotic capacitance, ΔC_1 the difference between DC-capacitance and C_1 and R_1 is added for the time constant of the capacitance variations. Those three elements form a model that produces a capacitor which has a decreasing capacitance with increasing frequency. [15]

With those parasitic elements, the divider starts to exhibit a phenomena in step response presented in figure 2.16. It can be seen that the "creeping" follows an exponential curve, just like a 1st-order system without time delay. Once the initial step is settled the measured quantity will start to rise slowly. This rise is upwards and only downwards when there is a compensation in the low voltage arm that has wrong sizing of component values.

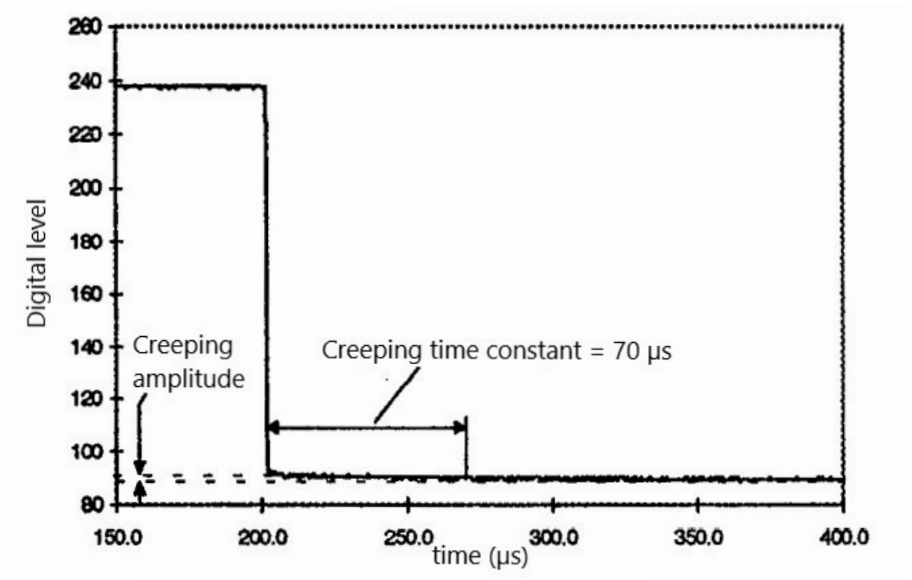

Figure 2.16. *Upward "creeping" of the step response. [15, edited]*

The divider of TAU is of a damped capacitive type as Li and Rungis [15] claim that is a divider type especially experiencing problems with "creeping". It is also stated in the paper that this can be corrected with measurements and an iterative process. The "creeping"

can be compensated by putting a similar RC-circuit as in figure 2.15 in parallel to the low-voltage arm's capacitor so the impacts of high-voltage and low-voltage sides cancel each other out. The process becomes iterative because the parameters used to calculate compensating components' values are hard to determine accurately due to noise level and inductances in the circuitry. [15]

The compensating elements' values are calculated from the step response and divider values. The "creeping" amplitude

$$\frac{\Delta V}{V} = \frac{\Delta C_1}{C_1 + \Delta C_1}, \tag{2.7}$$

where ΔV and V are the final voltage after "creeping" and voltage at the start of the "creeping". So i.e. the shift in voltage amplitude corresponds to the shift in capacitance value. The "creeping" follows an exponential curve as shown in figure 2.16 and this should equal to 1st-order time constant

$$\tau = \Delta R_1 \Delta C_1. \tag{2.8}$$

To compensate this "creeping", the low-voltage arm's capacitor needs to have parallel RC-circuit with the capacitance ratio being the same as in the high voltage capacitance ratio which should equal to the amplitude of the "creep" meaning

$$\begin{aligned} \frac{\Delta V}{V} = \frac{\Delta C_1}{C_1 + \Delta C_1} &= \frac{\Delta C_2}{C_2 + \Delta C_2} \\ &\approx \frac{\Delta C_1}{C_1} = \frac{\Delta C_2}{C_2}, \end{aligned} \tag{2.9}$$

where C_1 and ΔC_1 are the low-voltage capacitor's capacitance and compensating capacitor's capacitance. The equation 2.9 uses an assumption that the creeping amplitude is much less than the step amplitude i.e. the parasitic capacitance of the high-voltage capacitor in figure 2.15 is much smaller than the actual capacitance. There should also be a time constant in the low-voltage arm equal to the time constant of the high-voltage part. [15]

Using the previous equations 2.7–2.9 the values can be estimated. The values for ΔC_1, ΔC_2, ΔR_1 and ΔR_2 are

$$\Delta C_1 = \frac{\Delta V}{V} C_1 \tag{2.10}$$

$$\Delta C_2 = \frac{\Delta V}{V} C_2 \tag{2.11}$$

$$\Delta R_1 = \frac{\tau}{\Delta C_1} \tag{2.12}$$

$$\Delta R_2 = \frac{\tau}{\Delta C_2}. \tag{2.13}$$

From equation 2.10 the most interesting values are the values for ΔC_2 and ΔR_2 which is the compensating part added to the measuring system. The high-voltage equivalent values that are used to model the creeping are more interesting in a sense of simulating and understanding the phenomena but also if the initial correction is not fully compensating the "creeping" then to understand which direction to alter those compensating values. The final product should have ideally no creeping –i.e. a flat response– but this however cannot be fully met since the component values cannot be freely decided as there are only certain fixed component values available and the available physical space is limited so the parallel and series connection of the components to get a specific value is not an applicable option. Thus the compromise is not completely flat response or a bigger low-voltage arm in dimensions but latter might be not worth pursuing if there are other parts in the measuring system causing bigger errors than the partially corrected "creeping".

2.5 Uncertainty and traceability

The measurand is the value being measured. The measurand should have a well defined physical quantity that has a unique value. The resulting value obtained is only an estimate of the true value.

In history, the more known is the error analysis concept. Error means the difference of readings from the system under examination and the reference system. The system can be made better by compensating the single error contributions. When all the known error contributions are compensated the measured value still fluctuates if several measurements are taken.

Uncertainty is an estimate of a range within the true error of measurement lies, since the true error can't be ever exactly known. Therefore uncertainty does not have a positive or a negative sign. [16]

Measurement accuracy is important to know. While designing network components and doing withstand testing the component should be chosen to withstand specific voltages but if the measured voltage has large uncertainties the real voltage could be much more and the component should be chosen to keep that in mind. This results in increasing costs. Also it should be kept in mind that the accuracy – like performance checks of the measurement device regularly – also is expensive. [1]

Traceability of the measurement means an unbroken chain of measurements. This means that all the measured values can be traced back to the international SI-references. The measurement chain may consist of international comparisons of reference systems to national metering institute's measurements system to a testing lab's measurement system. This chain ensures that measurements performed in different countries and labs with different equipment and at different times and measurement conditions can be comparable

against each other. [1]

2.5.1 Errors and uncertainties

Let's assume that a measurand has a constant value of X_{true} in respect to time. Now the measurement of that value is affected by error sources as illustrated in figure 2.17. Errors may be caused for example by ambient temperature variations.

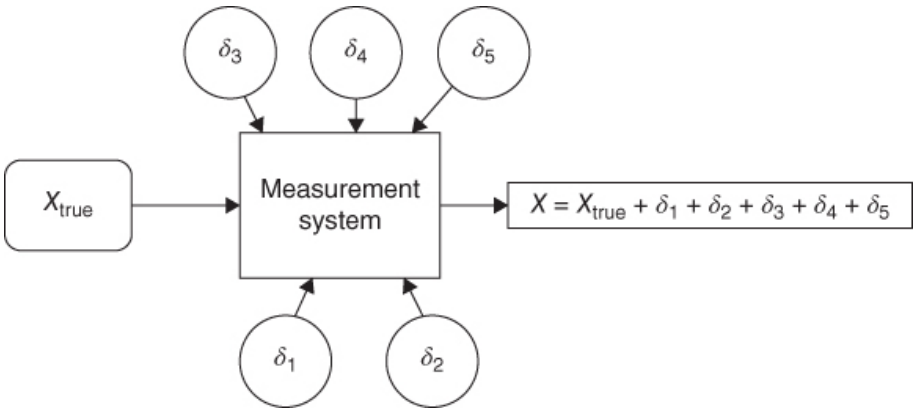

Figure 2.17. *Error sources [16].*

Now 2 consecutive measurements are taken from the measurand. The measured values

$$X_1 = X_{(true)} + (\sigma_1)_1 + (\sigma_2)_1 + (\sigma_3)_1 + (\sigma_4)_1 + (\sigma_5)_1 \tag{2.14}$$

$$X_2 = X_{(true)} + (\sigma_1)_2 + (\sigma_2)_2 + (\sigma_3)_2 + (\sigma_4)_2 + (\sigma_5)_2\,, \tag{2.15}$$

where X_1 and X_2 are the measured values and σ values are the errors. One notable thing is that $X_1 \neq X_2$. This is because some of the error sources vary during measurements and some remain constant. Now, designating the symbol β to be the error contribution that doesn't vary between the measurements and the ϵ to be the errors that do vary. The equation 2.14 reduces to

$$X_1 = X_{(true)} + \beta + (\epsilon)_1 \tag{2.16}$$

$$X_1 = X_{(true)} + \beta + (\epsilon)_2\,, \tag{2.17}$$

where $\beta = \sigma_1 + \sigma_2$ and $\epsilon = \sigma_3 + \sigma_4 + \sigma_5$.

In figure 2.18 is an example on how the errors add up to the real value. In (a) the illustration shows how the time-variant and time-invariant errors add up to the value obtained by

the measurement system. [16]

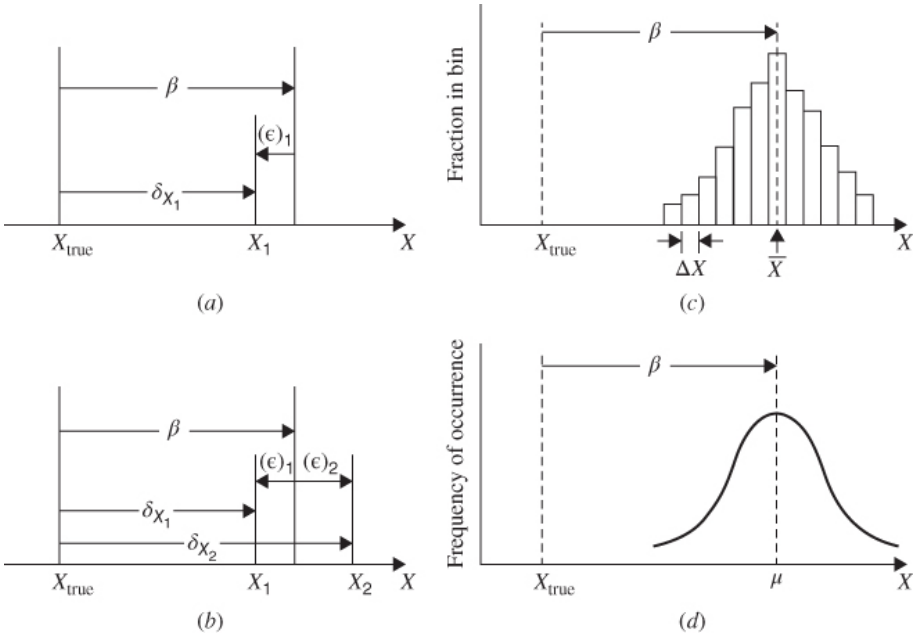

Figure 2.18. *Error effects [16].*

Figure 2.18a shows a single measurement. The β contains all the time-invariant errors and ϵ is the error that varies during every measurement. Figure 2.18b shows added second measurement after the first one. It can be seen that the β acts as an "offset" to the measurements. The total error σx varies because the ϵ is different for each measurement.

If enough measurements are performed, the ϵ values behave similarly to the histogram in fig. 2.18c. The mean value can be calculated and when moving away from the mean the number of measured values decrease. The standard deviation can also be calculated which represents the scatter of the measured values from the mean. If the measurements are continued infinite number of times the distribution of the measured values would look similar to 2.18d. [16]

2.5.2 Calibration

The scale factor of a LI measurement system is determined via intercomparison with a reference system. Both systems are fed with the same voltage and the output voltage is recorded. The scale factor of the system under test is

$$F_X = \frac{F_N V_N}{V_X}. \tag{2.18}$$

where F_N is the scale factor of the reference divider and V_N and V_X are the voltages measured by the 2 different systems. [2]

The voltage dividers are preferably set as in figure 2.19. The dividers are set symmetrically and with the same distance to the generator and walls. The high voltage lead should be similar and of similar length preferably. This however cannot always be achieved due to the limitations of the laboratory space. [6]

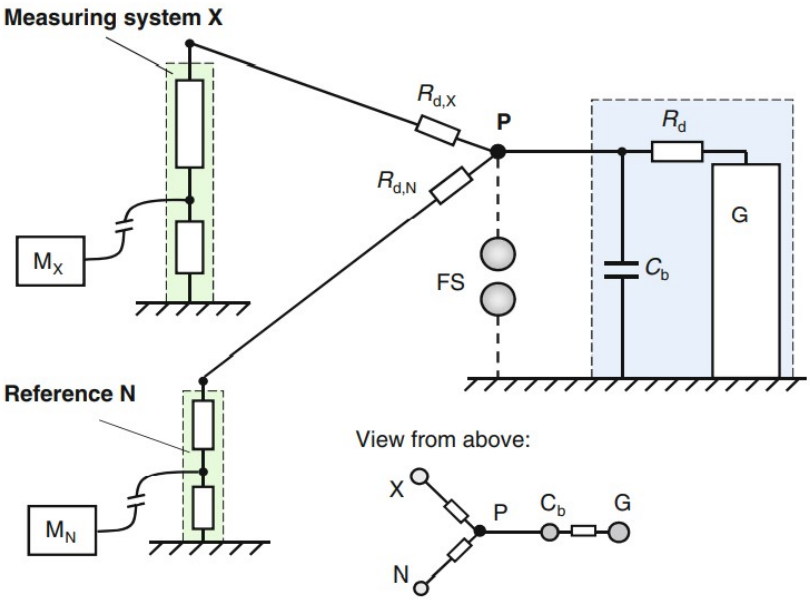

Figure 2.19. *Calibration setup with a reference divider [6].*

Usually the reference divider is smaller and cannot handle as high voltages as the divider under test. The standard [17] states that the comparison can be made using smaller voltages. Then an additional linearity test is needed to verify the scale factor and uncertainty at higher voltages than the voltages that reference system can handle. [1, 2] The latest IEC standard of 60060:2 states that the calibration range shall be 20 % or greater of the equipment's measurement range [17].

2.5.3 Uncertainty of a lightning impulse over voltage

The uncertainty means a parameter that shows the dispersion of measured values from the true value. The uncertainty depends on:

- quality of the measurement system under calibration
- the uncertainties of the reference system
- testing procedures used in the lab
- the effect of the environment (f.ex. temperature and near-by objects)
- measurement software
- measurement site (f.ex. earthing conditions)

- drift of the system
- measurement conditions (f.ex. relative humidity)
- measurement personnel (f.ex. reading errors). [1]

The calibration process will consist of multiple measurements. Multiple impulses on multiple different voltage levels are performed when the 2 systems are connected. The scale factor

$$F_g = \frac{1}{n}\sum_{i=1}^{n} F_{i,g} \tag{2.19}$$

is the mean value of *n* number of impulses. The symbol *g* denotes the voltage level used. [2]

If a Gaussian distribution is assumed, the relative standard deviation

$$s_g = \frac{1}{F_g}\sqrt{\frac{1}{n-1}\sum_{i=1}^{n}(F_{i,g} - F_g)^2}. \tag{2.20}$$

The standard deviation from the mean can then be calculated by dividing relative standard deviation with square root of n and this is also called the Type A uncertainty of that voltage level. Then the scale factor is derived from the mean values of different voltage levels used to record the impulses. The scale factor of system under calibration is

$$F = \frac{1}{h}\sum_{g=1}^{h} F_g \tag{2.21}$$

and the Type A uncertainty is the maximum uncertainty from the voltage levels selected. [2]

The nonlinearity of the determined scale factor is

$$u_{B0} = \frac{1}{\sqrt{3}}\max_{g=1}^{h}\left|\frac{F_g}{F} - 1\right|, \tag{2.22}$$

which means that the nonlinearity is regarded as a Type B evaluation. Type B uncertainty evaluation uses rectangular density distribution. It is assumed that all the different effects are of the Type B beside those that can be statistically determined ie. when there is small number of measurements in a series of measurements.

Usually the reference divider cannot handle as high voltages as the divider under calibration. The standard [17] states that the comparison of measurement systems can be then

performed by using a voltage level that the reference system can handle – needs to be at least 20 % of cabability of the system under test– and then complete the evaluation by a linearity test to apply that scale factor and uncertainties to higher voltages. In this case the scale factor

$$F = \frac{1}{a}\sum_{g=1}^{a} F_g, \tag{2.23}$$

where $a \geq 2$ is the voltage levels used in comparison to the reference measurement. The parameter $b \geq 2$ is the number of levels used in linearity test. The levels also need to be chosen that $a + b \geq 6$ is satisfied.

The type A uncertainty

$$u_A = \max_{g=1}^{a} u_g. \tag{2.24}$$

The Type A uncertainty is again the largest of the single standard uncertainties. The nonlinearity contribution is also similar to equation 2.22 but substituting h with a.

Impact of nonlinearity

When the system under calibration is bigger than the reference system and therefore calibration is performed only at a limited voltage range, the linearity test shows how the scale factor is valid at higher voltages. The estimation may be done f.ex. by comparing the measured voltage to the DC charging voltage at the input of the Marx generator circuit. The linearity test might show a different ratio from the scale factor but that is of no importance since only the stability of that factor over the whole voltage range is evaluated.

The ratio

$$R_g = \frac{V_X}{V_{CD}}, \tag{2.25}$$

where V_{CD} is the output of the comparison device such as a DC input of the Marx generator or a measuring gap. Now the Type B uncertainty for nonlinearity

$$u_{B1} = \frac{1}{\sqrt{3}} \max_{g=1}^{b} \left| \frac{R_g}{R_{mean}} - 1 \right|. \tag{2.26}$$

The figure 2.20 shows how the linearity test is performed. The a and b parameters are chosen to be 2 and 4 respectively.

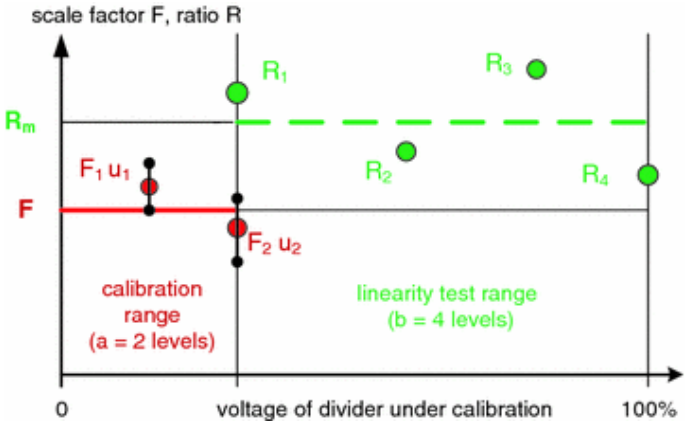

Figure 2.20. *Linearity test range [2].*

The voltage level where F_2 is recorded cannot be lower than 20 % of the rated voltage of the divider under test [4]. It can be seen from the figure also that the linearity test has a different scale factor and ratio readings but the deviation from the mean isn't significantly higher. This ensures that uncertainty of the equipment isn't too large. [2]

2.5.4 Dynamic behaviour

The type B uncertainty due to dynamic effects

$$u_{B2} = \frac{1}{\sqrt{3}} \max_{i=1}^{k} \left| \frac{F_i}{F} - 1 \right|, \tag{2.27}$$

where k is the number of the scale factor determinations. The scale factor is determined preferably via measuring the frequency response of the system or by a range of different shapes of impulses.

For the lightning impulse, the dynamic behaviour can be evaluated with setting the front time of the pulse to be at the $\pm$ 30 % limits and assume rectangular distribution. For a divider that is used in measuring AC voltages the divider is fed sinusoidal low voltage and the scale factor is measured while varying the frequency. [17]

2.5.5 Short-term stability

The uncertainty contribution due to the short-term stability is mainly due to heating of the converting device. This is due to resistive parts heating in the high voltage divider during testing. The scale factor is determined at rated operating voltage at the start of the testing and again when test time is over. The type B uncertainty regarding short-time stability

$$u_{B3} = \frac{1}{\sqrt{3}} \left| \frac{F_2}{F_1} - 1 \right|, \tag{2.28}$$

where F_1 is the is the scale factor at the start of the testing event and F_2 is the scale facter determined when the testing has been taken place. [2]

2.5.6 Long-term stability

The stability of the scale factor is usually evaluated by data provided by two most recent performance checks or by manufacturer's data. The Type B contribution regarding the long-term stability

$$u_{B4} = \frac{1}{\sqrt{3}} \max \left| \frac{F_2}{F_1} - 1 \right| \frac{T_{use}}{T_2 - T_1}, \tag{2.29}$$

where F_1 and F_2 are the scale factors of two performance checks made at times T_1 and T_2. The T_{use} is the projected time of use, which usually is $T_2 - T_1$. [2]

If the measurement system is relatively old ie. there are number of performance check data available then the Gaussian distribution can be assumed. Type A uncertainty contribution for the long term stability

$$u_{B4} = \frac{T_{use}}{T_{mean}} \sqrt{\frac{\sum_{i=1}^{n} \left(\frac{F_i}{F_m} - 1 \right)^2}{n - 1}}, \tag{2.30}$$

where F_i is the scale factor from a performance test number i, F_m is the mean scale factor of those performance checks and T_{mean} is the mean time difference between the performance checks. [17]

2.5.7 Ambient temperature

The scale factor of the measurement system is vulnerable to ambient temperature variations. To measure the uncertainty regarding ambient temperature, the scale factor is determined at different temperatures or calculated from the properties of the individual components in the system. The resulting Type B uncertainty

$$u_{B5} = \frac{1}{\sqrt{3}} \left| \frac{F_T}{F} - 1 \right|, \tag{2.31}$$

where F is the scale factor at calibration temperature and F_T is the scale at the considered temperature. The temperature correction factor should be used if the ambient temperature changes over 1 %. [17]

2.5.8 Proximity

The measurement system's scale factor changes due to proximity of earthed or energized structures. This might be via stray capacitances from divider to HV test laboratory's earthed wall and/or the Marx generator. The type B uncertainty

$$u_{B6} = \frac{1}{\sqrt{3}} \left| \frac{F_{max}}{F_{min}} - 1 \right|, \tag{2.32}$$

where F_{max} and F_{min} are the minimum and maximum distances to the nearby structures. [2] The u_{B6} might have a set of values for a set of distance ranges [17].

2.5.9 Software

The software effects on the captured waveform such as quantization error can be evaluated by feeding the program artificial test data. The software contribution to uncertainty is discussed in IEC 61083-2 standard.

The uncertainty

$$u_{B7} = \frac{1}{\sqrt{3}} \max_{i=1}^{n} T_{oi}. \tag{2.33}$$

The T_{oi} are the tolerance ranges for the artificial test data. The software effect only depends on that single value and is estimated similarly than the other contributions, by the type B estimation method. [6]

2.5.10 Combined uncertainty

The standard uncertainties evaluated by type A and type B methods can be combined and combined standard uncertainty

$$u_c = \sqrt{\sum_{i=1}^{N} |c_i u(x_i)|^2}, \tag{2.34}$$

where N is the amount of standard uncertainties $u(x_i)$ and c_i is the sensitivity coefficient, calculated.

The equation 2.34 applies only when the individual uncertainties have no correlation. if two or more uncertainties have correlation, extra steps need to be taken f.ex. estimating the correlation factor. [18]

2.5.11 Expanded uncertainty

In industrial measurement systems, the coverage probability needs to be 95 %. The expanded uncertainty

$$U = ku_c = \sqrt{\sum_{i=1}^{N} |c_i u(x_i)|^2}, \tag{2.35}$$

which reguires a value for coverage factor k. The coverage factor is typically 2.1 if the individual uncertainty contributions have good estimates. [6, 18]

If an approved measurement system is used in calibrating setup, the expanded uncertainty

$$U = 2\sqrt{u_{cal}^2 + \sum_{i=0}^{N} u_{Bi}^2}, \tag{2.36}$$

where k value of 2 is used to gain approximately 95 % coverage probability and u_{cal} is the uncertainty of the approved measurement system. The parameters u_{Bi} are the standard uncertainties of the type B contributions f.ex. linearity effect. [17]

2.6 Travelling waves

In case of transient phenomena – i.e. oscillatory behaviour during a short time span – a circuit analysis should be altered to match the phenomena. This is done via a distributed parameter network shown in figure 2.21. [10]

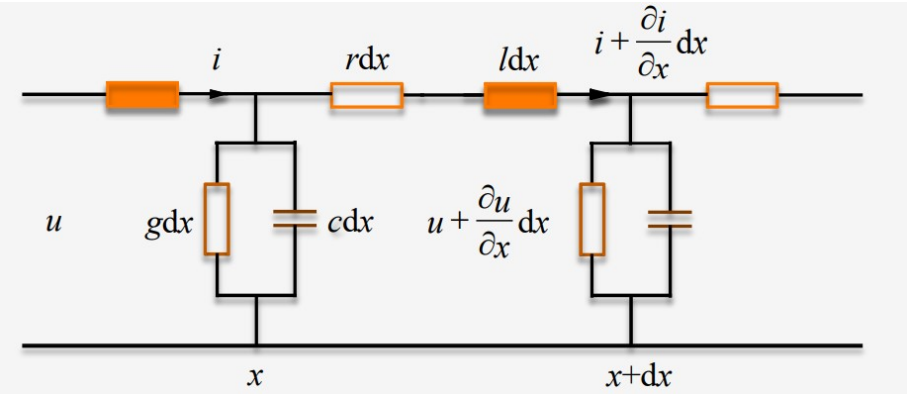

Figure 2.21. *A transmission line with distributed elements. [10].*

The impedance parameters in the figure mean impedances per unit length. If a wave travels to the positive direction on the x-axis, the voltage and current of the travelling wave along the line

$$u(t,x) = e^{-a\frac{x}{v}} f_1\left(t - \frac{x}{v}\right) + e^{a\frac{x}{v}} f_2\left(t + \frac{x}{v}\right) \tag{2.37}$$

$$i(t,x) = \frac{u(t,x)}{Z_w} \tag{2.38}$$

$$Z_w = \sqrt{\frac{l}{c}} \tag{2.39}$$

$$a = \frac{r}{2l} + \frac{g}{2c}, \tag{2.40}$$

where Z_w is the wave impedance off a lossless line, v the velocity of the traveling wave and f_1 and f_2 are dependent on boundary conditions like the initial voltages along the transmission line. [1]

Now from the previous the most noticeable thing to point out is the fact that wave velocity $v = 1/\sqrt{LC}$ is only dependent on the line parameters and not line length. Line length affects the travel time. If two lines with different paremeters and therefore different wave impedances Z_w are connected the lines will have different wave velocities. [19] For example a underground cable will have lower velocity for travelling waves than in an overhead line [10].

2.6.1 Reflections

When a traveling wave is crossing a discontinuity region, reflections occur to the receiving and sending end. If for example a cable changes to overhead line, the wave impedance increases. This results in incoming current to drop at the receiving end and a charge to accumulate in the transition region. This charge will increase the voltage at that point and the voltage will travel backwards. The result is that the traveling wave will hit the discontinuity region and from there the wave splits into two waves: reflected and transmitted waves shown in figure 2.22. [10]

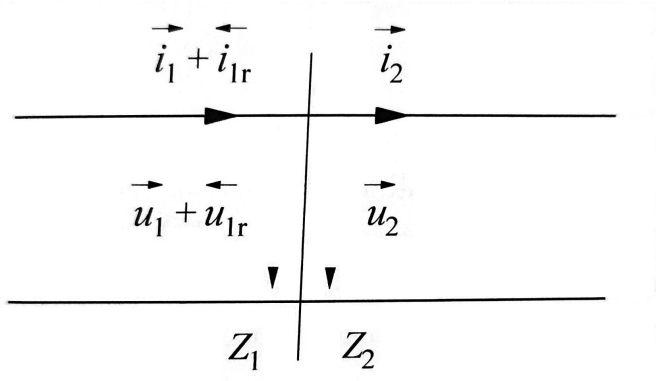

Figure 2.22. *Reflections in a wave impedance discontinuity region. [1]*

The balance conditions for the reflections are

$$u_1 + u_{1r} = u_2 \tag{2.41}$$

$$i_1 + i_{1r} = i_2. \tag{2.42}$$

The derivation of equations 2.41, 2.42 and figure 2.22 results in

$$u_2 = \frac{2Z_2}{Z_1 + Z_2} u_1 = \tau_u u_1 \tag{2.43}$$

$$u_{1r} = u_2 - u_1 = \frac{Z_2 - Z_1}{Z_1 + Z_2} u_1 = \rho_u u_1 = (\tau_u - 1)\, u_1 \tag{2.44}$$

$$i_2 = \frac{u_2}{Z_2} = \frac{2Z_1}{Z_1 + Z_2} i_1 = \tau_i i_1 \tag{2.45}$$

$$i_{1r} = i_2 - i_1 = \frac{Z_1 - Z_2}{Z_1 + Z_2} i_1 = \rho_i i_1 = (\tau_i - 1)\, i_1. \tag{2.46}$$

The ρ and τ are the reflection and transmission coefficients respectively. [1]

The equations 2.43–2.46 tell how the traveling wave energy divides between incident and reflected current and voltage waves:

- If $Z_1 = Z_2$, then the transmission and reflection coefficients both are zero and hence no reflection and the whole wave is transmitted.
- If $Z_2 = 0$, there is no transmitted energy and the incoming voltage wave is fully reflected with a negative sign
- If $Z_2 = \infty$, there is no transmitted energy and the incoming current wave is fully reflected which results in voltage doubling in the discontinuity region. [20]

Figure 2.23 shows an example where surge impedance of a transmission line changes to half of its original value. The coefficients for τ_u and ρ_u are 0,67 and -0,33 respectively.

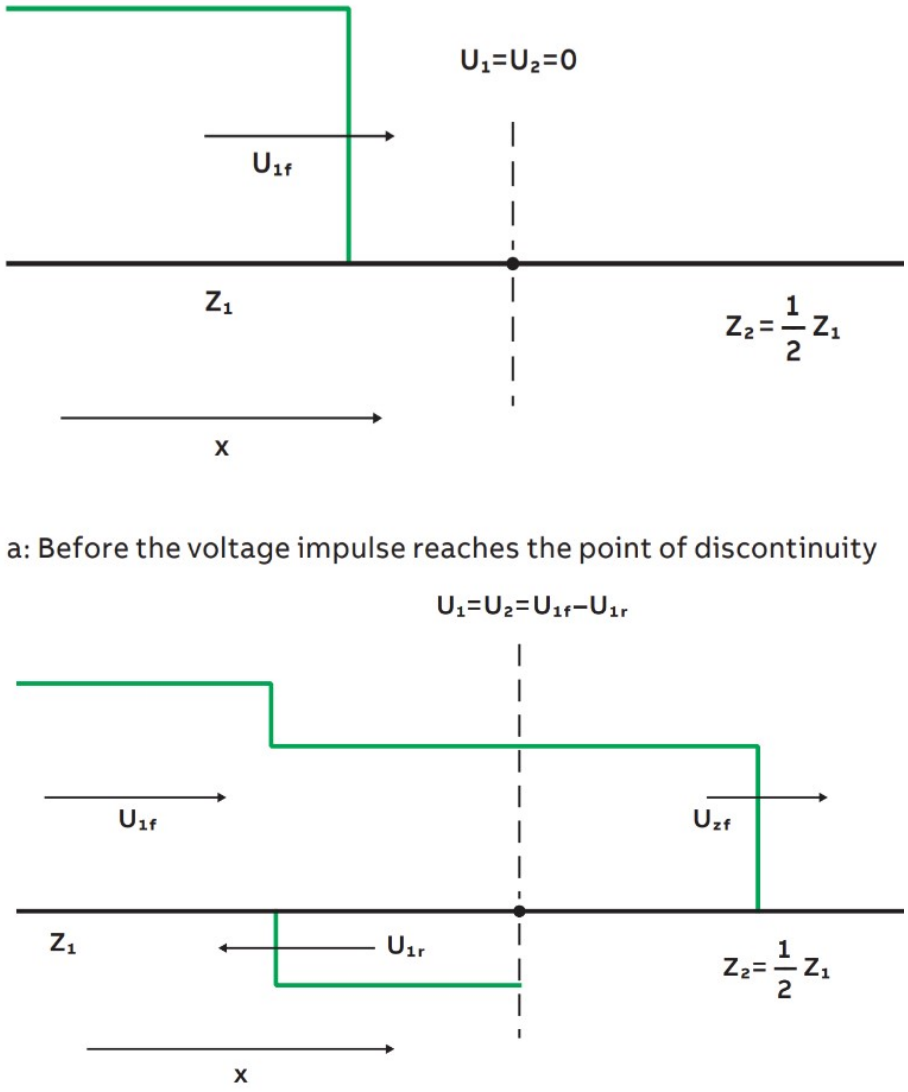

Figure 2.23. *Traveling wave in a point of discontinuity. [21]*

As can be seen from the figure 2.23, the incoming voltage wave is reflected and the reflected wave is superpositioned on top of the incoming wave. The transmitted wave is incoming wave minus the reflected wave. [21] This superspositioning principle can be used for analysing also more complex waves [1].

2.6.2 Series impedance matching of a cable

As discussed in chapter 2.6.1, the reflections wont occur if $Z_2 = Z_1$. Considering the voltage divider and its coaxial or triaxial measurement cable with a wave impedance of 50 Ω to the control room with measurement device such as a oscilloscope with 1 MΩ resistance. Since the difference is so high the measurement device can be assumed to have infinite resistance. From that assumption the figure 2.24 is formed.

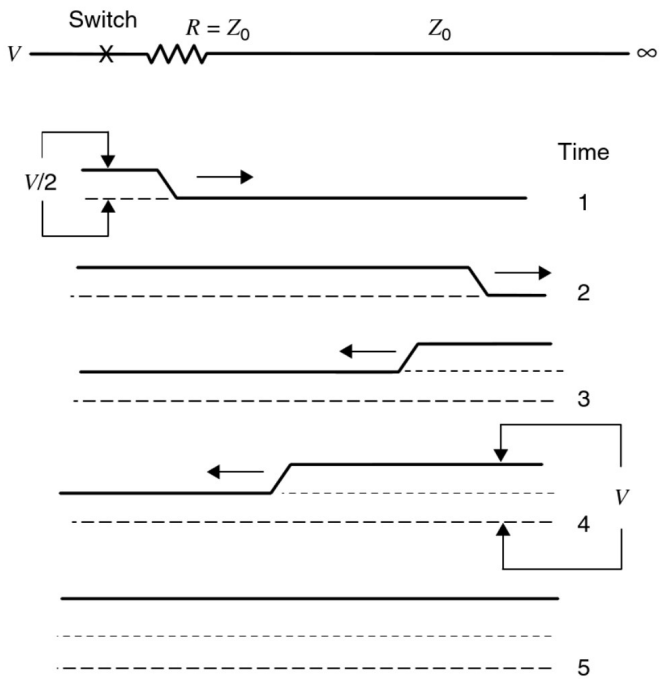

Figure 2.24. *Series terminated transmission line. [22]*

As the switch in the circuit operates the voltage that propagates along the coaxial cable is $\frac{V}{2}$ because of the terminating resistor and the resistance of the line in series. As the end of the cable is considered as an open circuit, the whole wave is reflected back. The reflected wave is superpositioned on top of the incoming wave and when the reflection reaches the source terminal, the voltage is V along the whole system. When the whole system has reached this state there is no missmatch of charges so there wont be any additional reflections and the whole wave phenomena stops. [22]

Therefore it is beneficial to introduce a series terminating resistor to terminate the reflections in the long measurement cable of a LI measurement system. A full terminated mixed divider is shown in figure 2.25.

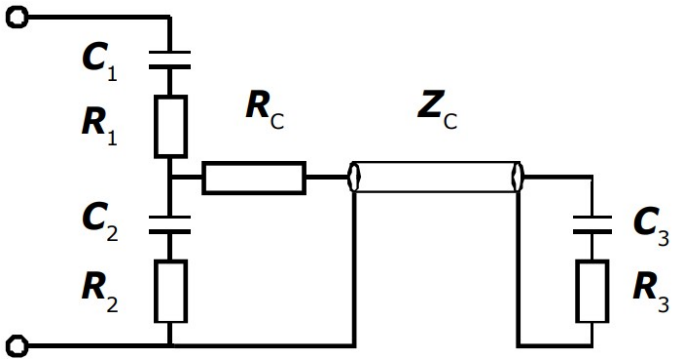

Figure 2.25. *Fully terminated mixed divider. [8]*

The R_C should be equal to Z_C as discussed earlier. This will terminate most of the

unwanted ringing. Usually the mixed divider is only terminated with R_C. In that case $R_C = Z_C - R_2$. When a fast transient is reflected and travels to the low voltage arm it is absorbed by the series connection of R_C and R_2. [8, 11]

It needs to be noted that this version does not eliminate all of the reflections. This is because $R_C \neq Z_C$ so the input voltage doesn't divide equally among those parts. For better results a part of the terminating resistor should be placed in the measurement end as shown in figure 2.25. There are several methods to determine the sizing of the components discussed by Yu et al. [23]. Problems arise when the measurement cable is so long that the $C_2 \gg C_K$ condition is not met or there are parasitic inductances causing LC oscillations [23].

One solution to design the matching parameters is that

$$\begin{cases} R_3 \approx 8.5 Z_C \\ C_3 = \frac{Z_C(C_1+C_2)}{R_3} - C_K \end{cases}, \tag{2.47}$$

where C_K is the capacitance of the cable [8]. As can be seen from equation 2.47, the parameter C_3 is greatly dependent on the cable's length i.e C_K's value.

2.7 The oscilloscope

The first oscilloscopes used in high voltage pulse measurements were cathode ray oscilloscopes. In the 70's a digital oscilloscopes were introduced. [24] Each oscilloscope possesses different characteristics that makes an oscilloscope more or less suitable for a different type of measurements, like fast transients.

The step response is a fast transient occuring in a sub 1 µs timeframe. To capture this the oscilloscope should have a bandwidth high enough to be able to detect the the signal being measured and all the oscillations superimposed to the signal. If the bandwidth is too low, all the details in the waveform cannot be correctly recorded such as sharp edges. The general "rule-of-thumb" is that the scope should have 5 times or higher bandwidth than the fundamental signal being measured so that the first harmonics in the signal can be captured.

Other important parameter regarding an oscilloscope is the rise time. Fast rise time is needed to capture fast transitions and also for accurate time measurements. Rise time is usually defined as a ratio of $\frac{k}{Bandwidth}$, where k-parameter is about 0.3–0.4 depending on the model of the oscilloscope. Rise times are critical when measuring especially square waves. [25] The rise time of the measured pulse in square wave setup with a voltage divider is in a few nanoseconds due to a mercury-wetted relay having such fast operating time. So if the oscillations during the rising edge need to be recorded accurately, a rise

time of few hundred picoseconds need to be achieved by the oscilloscope.

If the oscilloscope is a digital oscilloscope so the signal is run through an attenuator or an amplifier before digitizing the signal via analog-to-digital converter as can be seen from fig. 2.26. These attenuators or amplifiers determine the scale seen on the display. These attenuators also distort the signal uniquely. Also the different input channels might not behave the same way due to for example component tolerances in the circuitry and stray impedances.

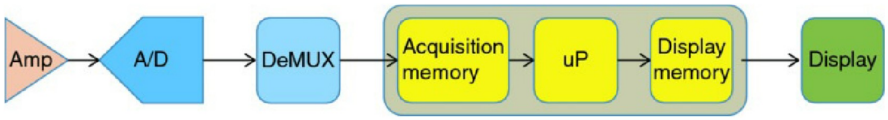

Figure 2.26. *Architecture of a digital oscilloscope. [24]*

3. ANALYZED MEASUREMENT SYSTEMS

TAU's measurement system consists of a damped capacitive divider, a measurement cable and a digitizer. The VTT's digitizer can be used with the same divider and that has a fiber optic link to the control room so a short measurement cable can be used.

There are three instrument combinations studied. The first system is TAU's old system with the old LVA is the complete system made by a manufacturer. The second system is TAU's new system which introduces a new measurement cable and LVA. The third system is TAU's new system but with VTT's digitizer that has a built in correction software.

3.1 Lightning impulse measurement system of TAU

The TAU's 1 MV lightning impulse voltage measurement system consists of a damped capacitive type of voltage divider made by Haefely. The model is CS 1000-670 which means that the model is suitable for measuring 1 MV of LI as well as 750 kV of SI.

The column is assembled with 3 pieces of 2 nF capacitors and a 230 Ω damping resistance all connected in series and the complete structure is 3.6 meters tall as shown in fig 3.1. The divider is standing on a steel support that has insulator support structure to separate the lowest HV capacitor from ground. The lowest HV capacitor stands on a large steel plate which might be problematic when considering stray capacitances of the system.

Figure 3.1. *TAU's damped capacitive divider.*

The old low voltage arm shown in fig. 3.2 is connected to the column via big plate-like structure to the HV capacitor's bottom terminal by the compressive force provided by the threaded rods and wing nuts. The capacitors and resistors are of a through-hole type components connected to belt-like intermediate terminals. The matching resistor for the 75 Ω cable is inserted in the middle of the LVA. The LVA is connected to coaxial cable that travels to the digitizer in the control room.

Figure 3.2. *TAU's old low voltage arm.*

The digitizer is also from the same manufacturer. The model is DIAS® 733 which has 100 MS/s sample rate and 2 input channels. There's an automatic evaluation of the waveform based on the chosen evaluation method such as chopped LI. The evaluation is based on the latest standard.

The input channel has a maximum voltage of 2 kV. The voltage from the coaxial or triaxial cable is further attenuated with a 1:200 attenuation ratio to be suitable for the equipment. The waveform is then digitized with a 10-bit system. [26] The attenuator will have some unidealities like temperature dependancy that will have an impact on uncertainty also besides the software contributions caused by f.ex. digitizing.

3.1.1 New lightning impulse measurement system of TAU

The first design of a new low voltage arm is shown in figure 3.3. The design features a printed circuit board with the low voltage resistance and capacitance divided to it to achieve coaxial layout. The matching resistor is connected to the circuit board through the middle of the board and the other end is connected to a triaxial cable connector. The triaxial cable is used to shield the innermost conductor from interferences. A measure has also been taken to protect the circuit from overvoltages by a protection component in the backside of the circuit board.

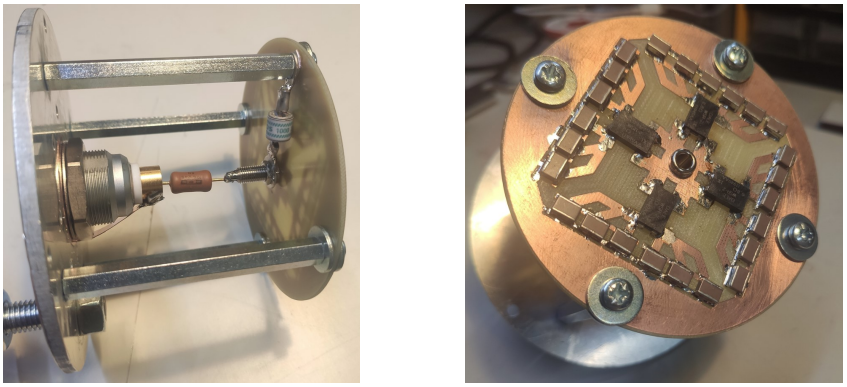

Figure 3.3. *First version of the new LVA.*

The low voltage arm components are separated from the high voltage capacitor be with a plastic housing structure, the high voltage part is connected to the low voltage part's circuit's HV side via a banana connector. The connection to the triaxial signal cable is shown in figure 3.4.

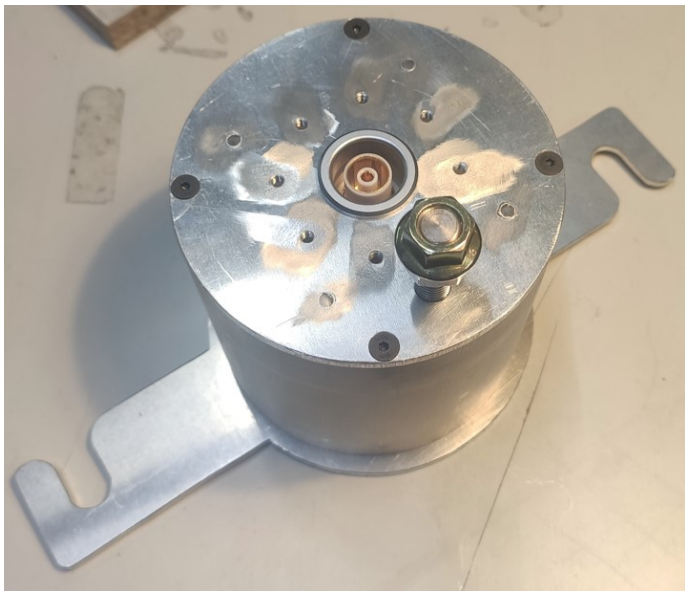

Figure 3.4. *First version of the new LVA, fully assembled.*

The resulting device has a few disadvantages. Those are mainly due to stray capacitances from HV to circuit board's ground electrode and a bit large inductive loop.

3.2 VTT's Digitizer

Reference system –VTT's HUT-400 divider– has a short coaxial cable and National Instruments PXIe-5164 digitizer with optical fiber connection to control room. The digitizer is shown in figure 3.5.

Figure 3.5. *NI PXIe-5164. [27]*

The sample frequency used for measurements is 200 MS/s and A/D resolution is 14 bits. Step response is corrected with a software. Figure 3.6 shows the step response of the NI

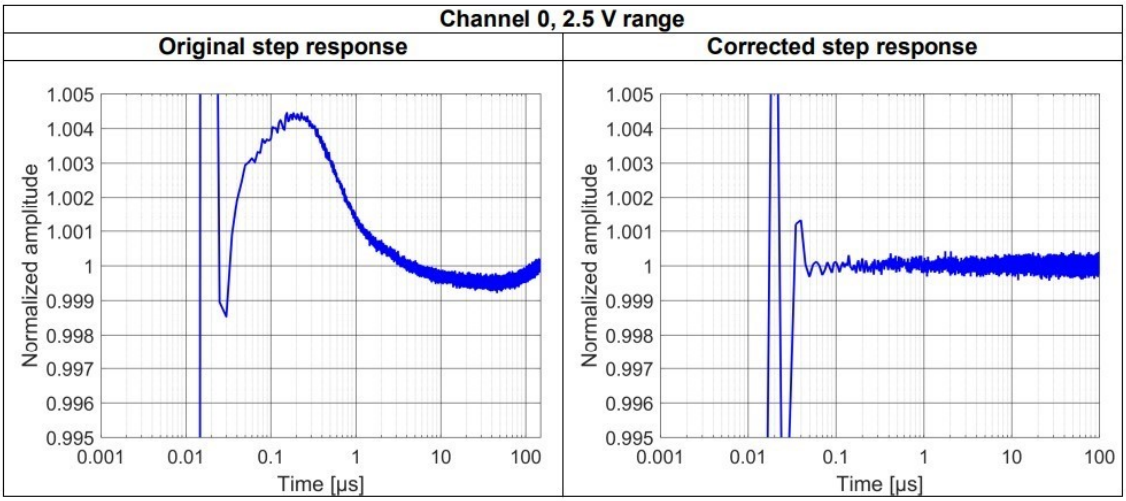

Figure 3.6. *Digitizer's step response before and after correction by convolution programm. [28]*

digitizer before and after the correction.

As can be seen, while using the 2.5 Volt measurement range, the step response of the digitizer is unideal but after the correction by software as discussed in chapter 2.7 the result is quite ideal. The first transient causes some overshoot and undershoot but that can be neglected since it lasts only the first 0.3 µs.

The digitizer is equipped with a short measurement cable to minimize the long cable phenomena. Therefore the digitizer needs to be set near the divider. Shorter cable will squeeze the travelling wave phenomena to the start of the step transient i.e. to the frequencies so high that it won't cause big distortions in the LI point of view. To overcome the interference effects due to nearby objects like the divider, the digitizer is also shielded using a grounded metal box.

The cable is connected to the digitizer via a 101:1 attenuator. The attenuator has a 1 MΩ input resistance and can withstand 2 kV of voltage. Usually the simple resistive attenuators are inaccurate at high frequencies due to stray capacitances parallel to the resistors. This can alter the attenuator ratio when entering high frequencies. To solve this a 20 pF of compensation capacitance is added parallel to the resistance. [29]

The step response for the attenuator is shown in figure 3.7. The ringing in the attenuator's step response will get damped after 300 ns so it is suitable for measuring fast transients. The creeping of the attenuator is much less than 0.1 %.

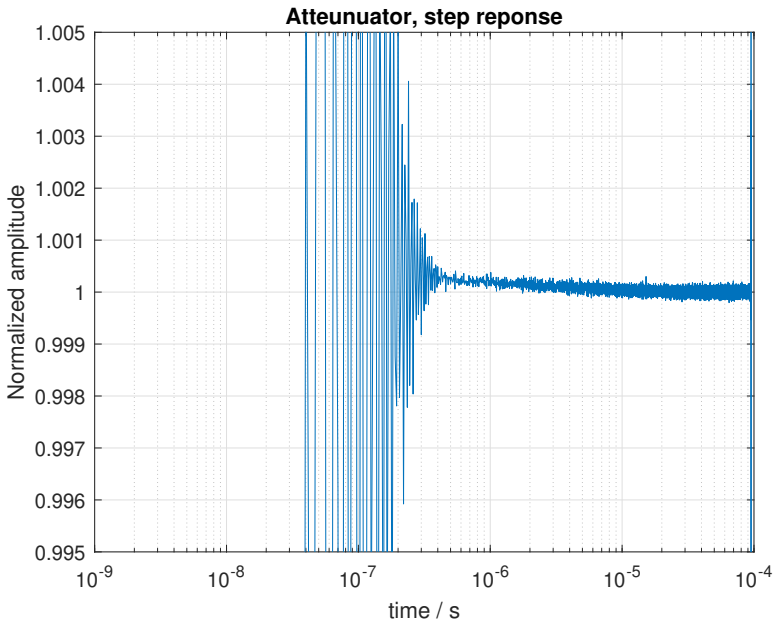

Figure 3.7. *Attenuator's step response.*

3.3 Oscilloscope correction

The oscilloscope's step response was measured with a mercury-wetted relay directly at the input channel and a lab power supply. The relay connected the power supply to ground. With averaging 100 identical steps –to reduce noise in the signal– a following result was obtained that in fig. 3.8.

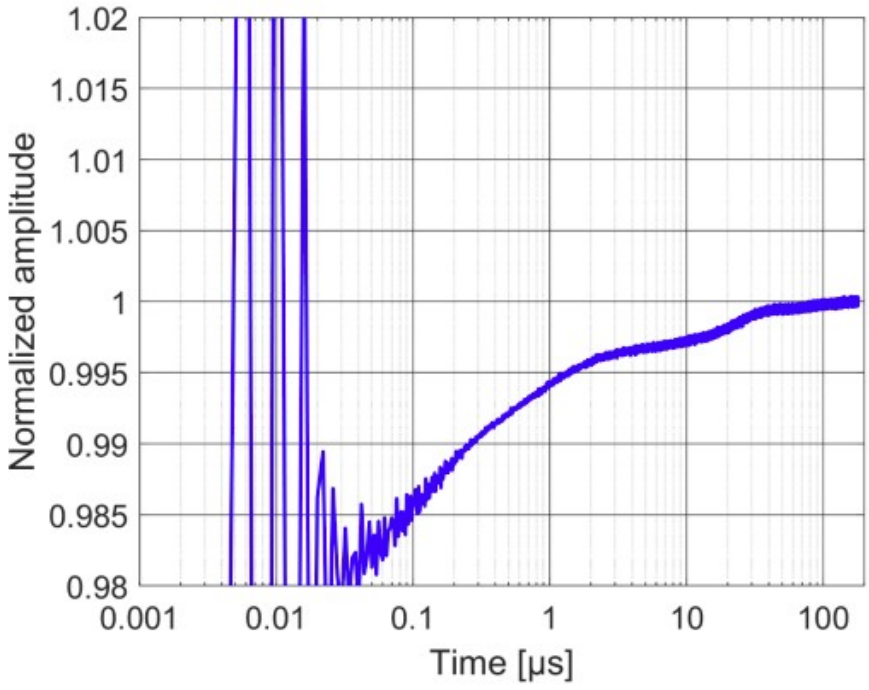

Figure 3.8. *Oscilloscope's response to a step signal. Channel 1, 50 mV/div.*

As can be seen from figure 3.8, the oscilloscope itself causes some drifting or "creeping" also. The different scales have unique responses due to different attenuators, so all the scales should be measured. The response recorded should be corrected with the knowledge of the oscilloscope's drift to minimize the effect of the oscilloscope.

This can be done via VTT's step correction program that uses a deconvolution approach to correct nonideal impulse. Although the program is intended for impulses, a square wave can be also corrected with it. Figure 3.9 shows how the program works.

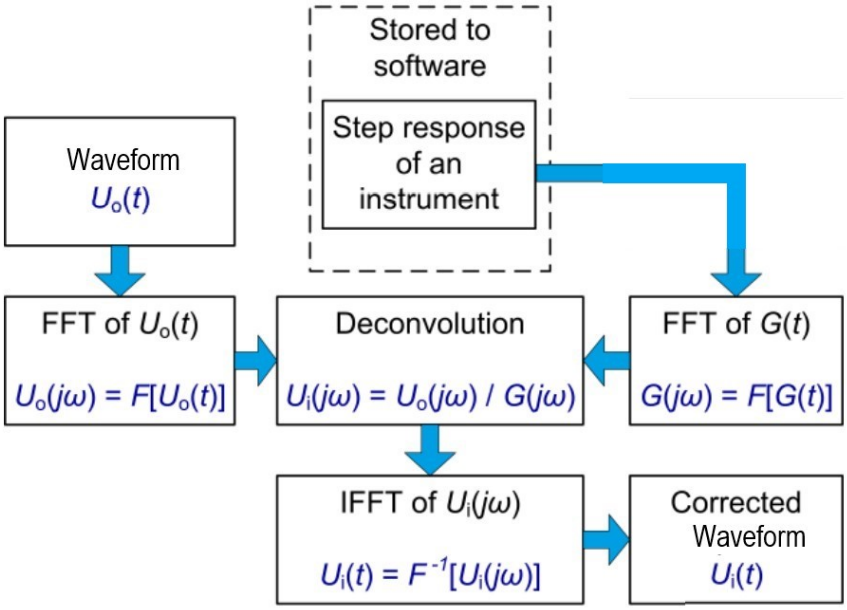

Figure 3.9. *VTT's deconvolution program. [30, edited]*

At the start the program chooses the channel and range from a set of ideal step responses recorded with those channel and range settings. The waveform that is needed to be corrected is then given to the program. The sample rates should be equal, otherwise the deconvolution won't work properly. Both waveforms are then transferred from time- to frequency domain with a Fourier transform. Now each frequency of the input signal is divided with the ideal –or almost ideal– and same frequency component of the recorded step response of the instrument. The result then is needed to convert back to time domain with inverse Fourier transformation. [30] The result should now have the step response of the divider only and and not the response of divider and the oscilloscope anymore.

4. IMPROVEMENT OF THE MEASUREMENT SYSTEM OF TAMPERE UNIVERSITY

The new low voltage arm has been built for the measurement system. The measurement cable has been switched from coaxial cable to triaxial. The new system uses the same digitizer and high voltage arm as the existing old system.

The new system needs tuning of the parameters inside the low voltage arm. Mainly to match the resistive and capacitive scale factors by changing the low voltage resistance. The compensation circuit is added to the new low voltage arm's PCB in order to improve divider's ability to measure T_2 correctly. Also the new system has a faster response so the oscillatory behavior in the step response needs to be minimized.

4.1 Improvements of the first version of the low voltage arm

The first version of the low voltage arm was designed to achieve a faster step response of the system as well as to have the option to fit compensation elements. The old, original, low voltage arm had components of a through hole type connected together coaxially and the matching resistor was placed to the middle.

The new low voltage arm had a PCB layout. The housing was similarly of a plastic tubular type. The new LVA design was more compact so the compensation can be fitted inside.

4.1.1 Inductive loop minimization

As can be seen from the figure 3.3, the circuit board's ground is connected to triaxial connector's ground via the four supporting beams. This loop –especially during fast transients like step response's rising edge– will cause a large disturbance via inductive loop of the support beam structure. The equivalent circuit can be seen in fig. 4.1 and if the mixed capacitive divider is experiencing a fast transient the LVA capacitance can be simplified as a short circuit and the whole divider's LVA is resistive.

If a voltage wave enters the resistive shunt i.e. the resistance of the LVA, the measurement cable experiences this plus the induced voltage that depends on the inductive loop

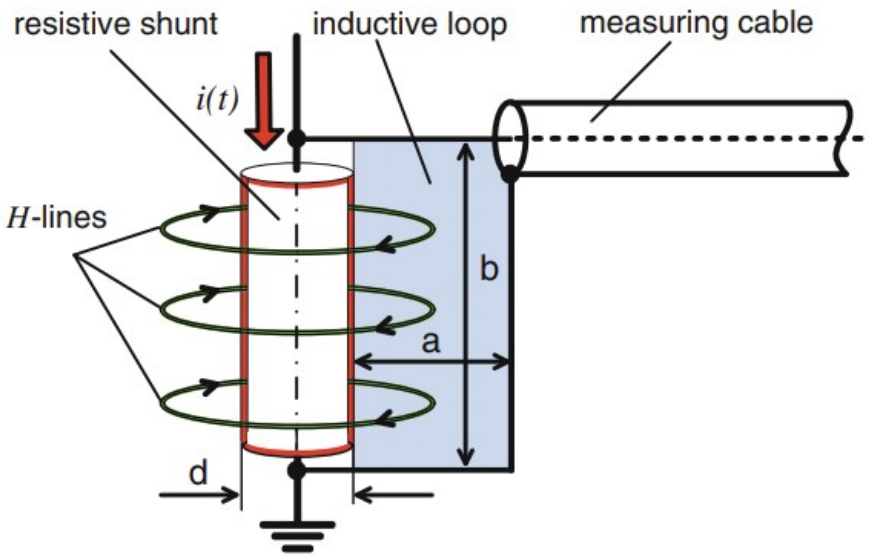

Figure 4.1. *Equivalent circuit. [2]*

parameters. The measured wave

$$\begin{aligned} v_m(t) &= v_R(t) + v_L(t) \\ &= R_m i_m(t) + L_m \frac{di_m(t)}{dt}, \end{aligned} \tag{4.1}$$

where v_m, v_R and v_L are the measured, resistive and inductive voltages of the circuit and R_m and L_m are the resistance and inductance of the circuit. To minimize the induced voltage that superimposes onto the resistive voltage, the loop has to be minimized since that loop size affects the L_m value.

Figure 4.2 shows how the loop size was minimized. Copper slips were inserted to make the loop smaller. Before the loop size alteration, the current path was through the steel beams that support the circuit board. Now the current path changes completely to through the copper slips because also plastic bolts and washers are used to insulate the support beams from the circuit board's ground.

Figure 4.2. *New LVA with loop size minimized.*

The results for loop minimization is presented in figure 4.3.

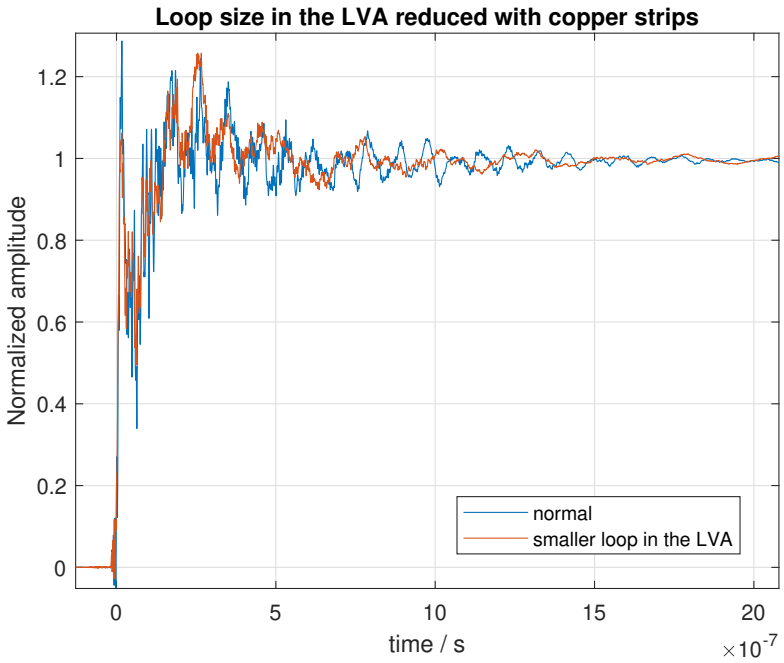

Figure 4.3. *Step response with loop size minimized.*

As can be seen the figure, the oscillations still remain. Some of the oscillations are more damped around the 600 ns. This loop reduction technique only helps so little that

the change is almost unnoticeable. This result excludes the scenario that the unideal behavior is due to the relatively large inductive loop formed by the support beams.

4.1.2 Different grounding improvements

The divider is normally set in the middle of the lab. The nearest ground mesh connection is approximately 1 meter away from the normal divider location.

The connection from low voltage arm is made via a copper braid to the supporting structure which has a wide copper strip to the grounding point in the lab's floor. The grounding point is in practice a copper pole going through the concrete floor surface layer and brazed to the continuous copper plate laboratory grounding inside the floor. This point from copper strip to the pole like structure serves as a wave impedance discontinuity point and may thus lead to unwanted reflections.

The different grounding point used was the same as the impulse generators grounding point. The grounding copper was extended to another grounding point at the laboratory's ground mesh. The new grounding point could have better conditions in terms of wave impedance and lower impedance connection contact to ground.

A star-type grounding mesh was built on top of the floor using approximately 10 cm wide copper foils. The new grounding system was connected to the laboratory ground from another point with possibly better impedance conditions.

Other issue with earthing is the measuring cable grounded at the control room. The control room connection to the lab's ground mesh might not be ideal. To achieve better grounding a braided copper mesh was pressed against the connector ground and other end was connected to the laboratory's grounding point.

Both of the grounding studies resulted in no improvement.

4.1.3 Capacitive coupling effects

The measured step response of the divider shows a significant peak. This is shown only with the new LVA, but that may be due to different capacitors in the low voltage arm. The stray capacitive coupling to the bottom of the HVA connects from the HV copper lead since the bottom support for the HV capacitors is large in area.

To shield against capacitive coupling, an earthed structure is placed above the lowest terminal of the HVA. The metal sheets used are separated from the terminal by wood acting as an insulating material. The sheets are grounded with a short, 5 cm wide, copper foil. The setup is shown in figure 4.4. The figure shows only the other half of the whole shielding plate setup. The setup without shielding can be seen from the fig. 3.1.

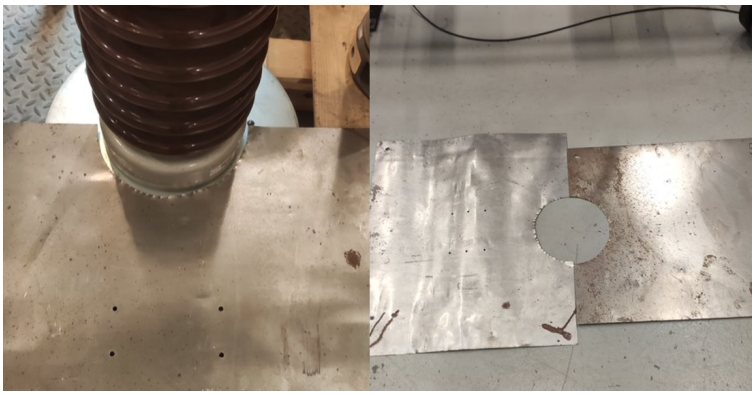

Figure 4.4. *Two steel plates to shield from capacitive coupling.*

In circuit simulations, with SPICE compatible program called Micro-Cap 12, the capacitive coupling can be seen as a capacitor connected from voltage source to the terminal which connects to measurement cable as seen in fig. 4.5. The output voltage over R7 resistor is plotted in figure 4.6 with a simulation step size of 2.5 ns.

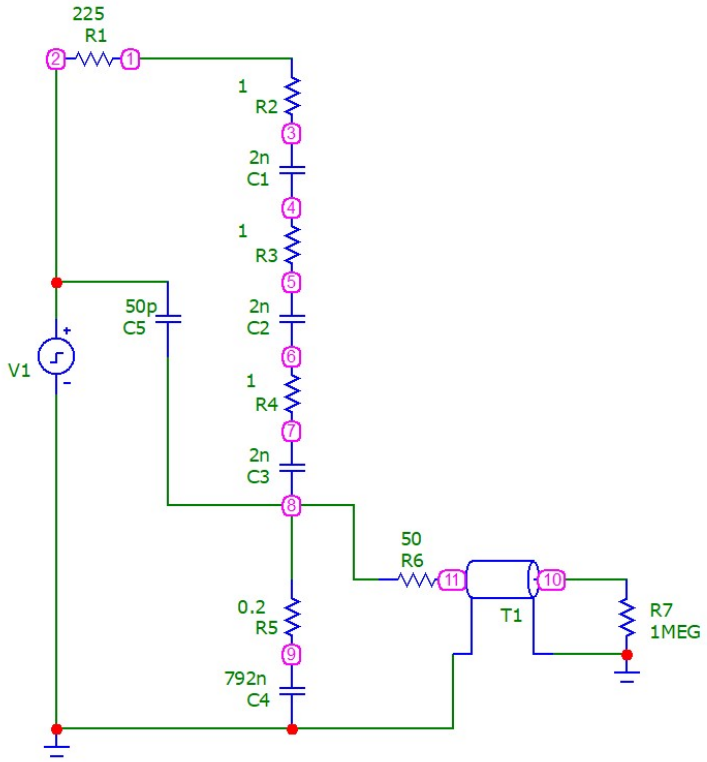

Figure 4.5. *Circuit of the capacitive coupling situation.*

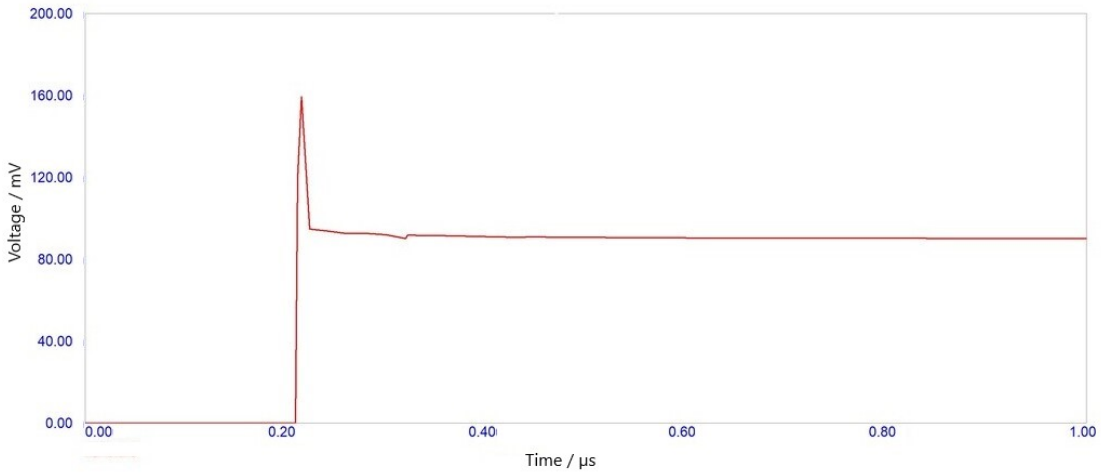

Figure 4.6. *Simulation case of the capacitive coupling.*

If the stray capacitance is 50 pF the step response will have over 50 % of overshoot. The small notch near the 400 ns mark is due to LVA resistor adding up to the cable terminating resistor i.e. $50\Omega \neq 50\Omega + 0.2\Omega$. This notch is relatively small though. That phenomena occurs after two times the travel time of the cable.

The results from step response tests are shown in figure 4.7. The initial peak isn't reduced but some of the ringing is damped more near the 0.5 µs mark. The results are otherwise very similar to each other.

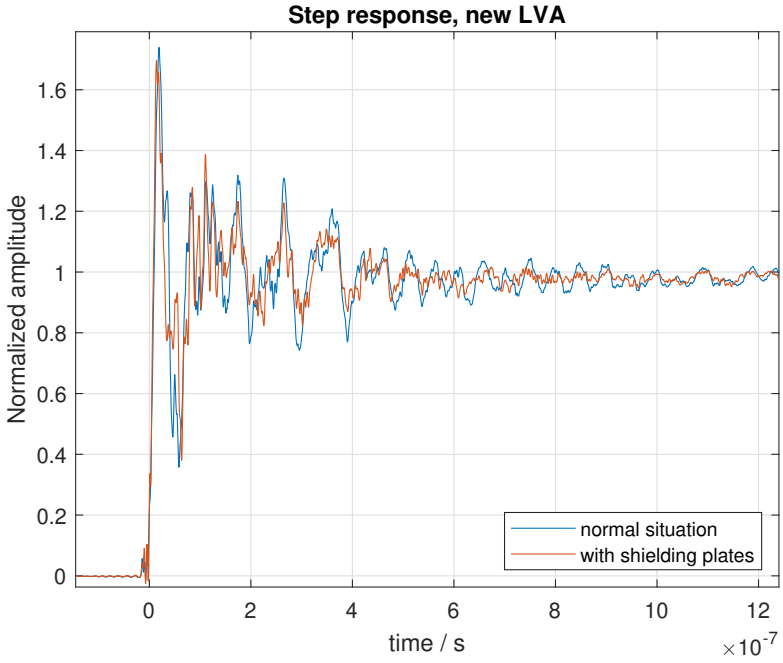

Figure 4.7. *New LVA with shielding against capacitive coupling.*

According to the simulations, the initial peak is due to the capacitive coupling from the

high voltage lead directly to the top of the LVA. However, the shielding doesn't improve the step response notably. This suggests that the initial peak isn't caused by this stray capacitive coupling.

4.2 Second improved low voltage arm design

The previously described LVA design had some unideal properties. The connection terminal that connects to the HVA is quite large and has some stray capacitance to the circuit board's ground. Other notable thing is the current loop size.

To minimize the loop size and loop's inductance as well as to improve the protection against stray capacitive coupling, a new LVA is constructed. The design is shown in the figure 4.8. A metal block is milled to fit the connector and PCB. The ground connected solid metal housing needs to be separated from the HV capacitor. This is done via an insulating plate that has copper on the other side and a feed through hole connection. This plate prevents capacitive coupling over the RC circuit of the LVA.

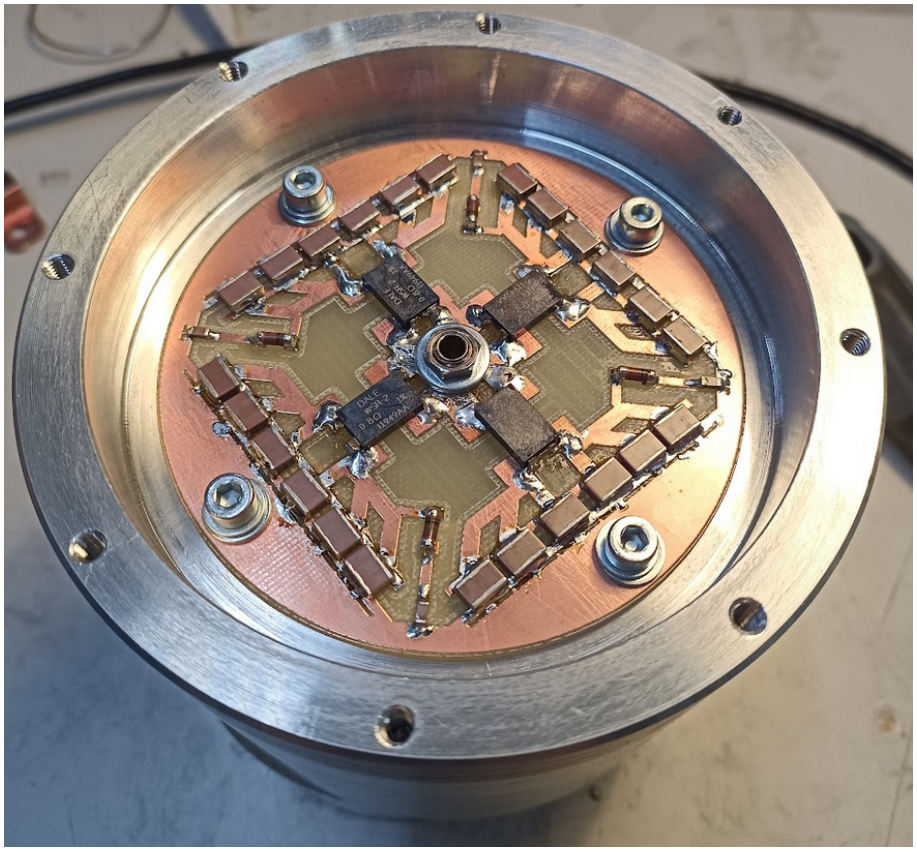

Figure 4.8. *Second version of the new low voltage arm.*

The measured step waveforms for the first and second housing of the new LVA are shown in fig. 4.9.

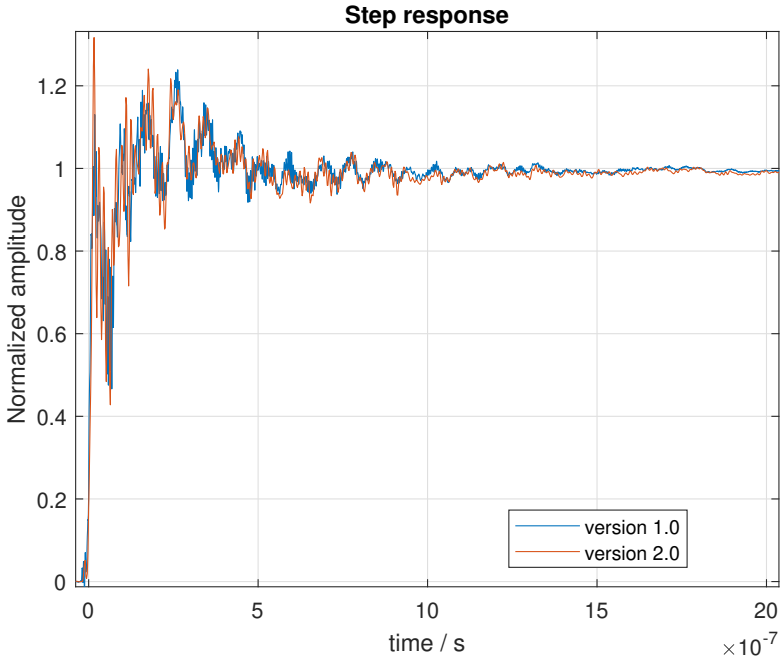

Figure 4.9. *Step responses of the both new LVA versions.*

The low voltage arm versions seem to behave similarly regarding the front time. The most noticeable difference is the initial peak. The peak on the start is a bit higher in the newer version. This might be the caused by the averaging of 50 pulses, if the trigger level is set in a place, where oscillations occur, the peak is reduced a bit. Both LVAs have similar peak at the start and then a significant drop to 75 % of the unit level and then rise back to the unit level.

4.2.1 Compensation branch in the low voltage arm

The divider of TAU is of damped capacitive type. Especially this type has been reported to be more likely to be influenced by creeping phenomenon [15]. The old measurement system showed significant creeping that resulted in relatively large error for the time parameters. The creeping phenomena was simulated and later also compensated in the new low voltage arm.

In the figure 4.10 there's a simulation example and it's corresponding circuit in figure 4.11 using approximately the values of TUNI's divider. Step voltage generator has a fast 0 to 300 Volt square wave inserted. The measured creeping can be seen to be about 3 % with τ being 20 microseconds.

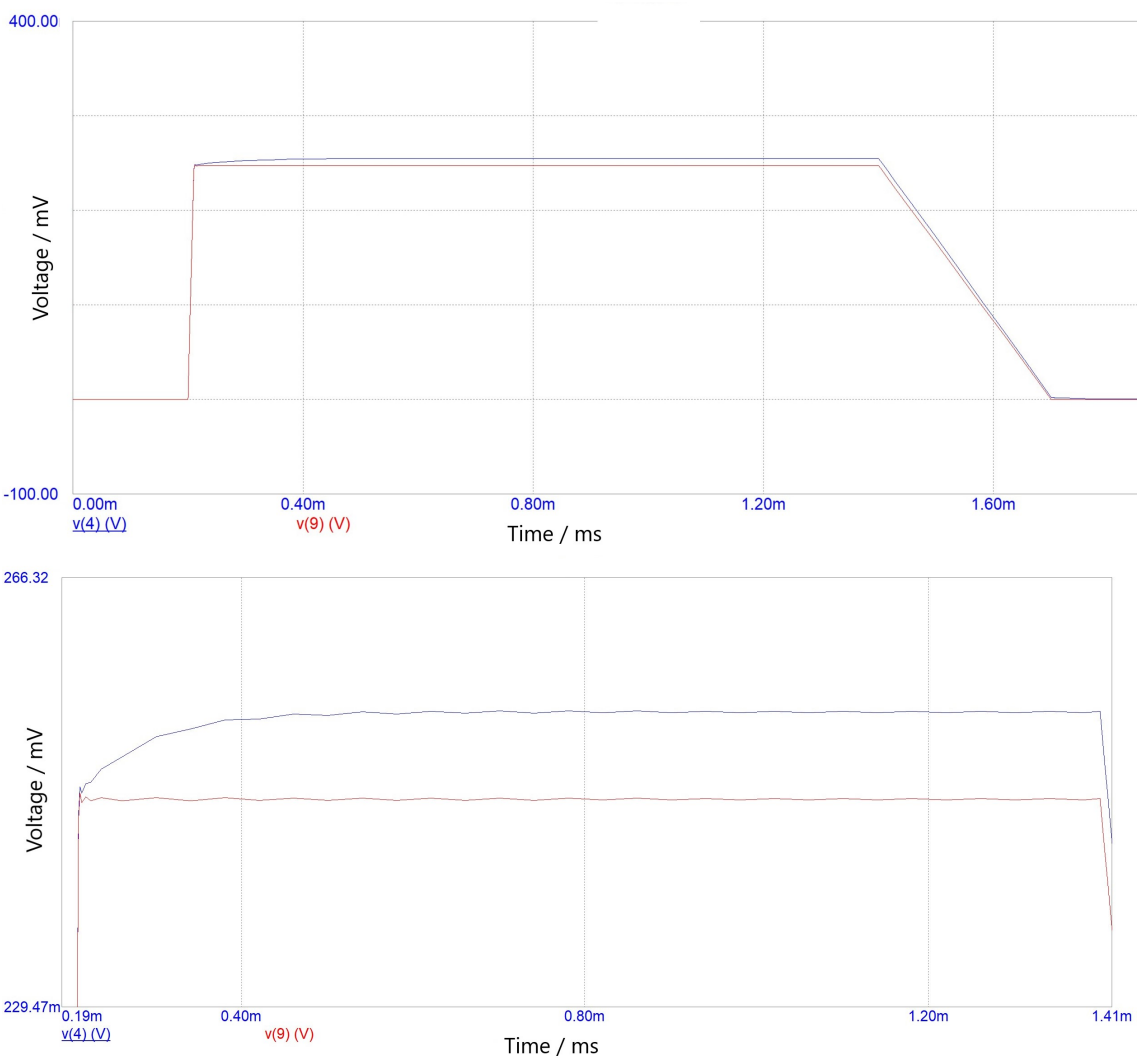

Figure 4.10. *Simulation of "creeping".*

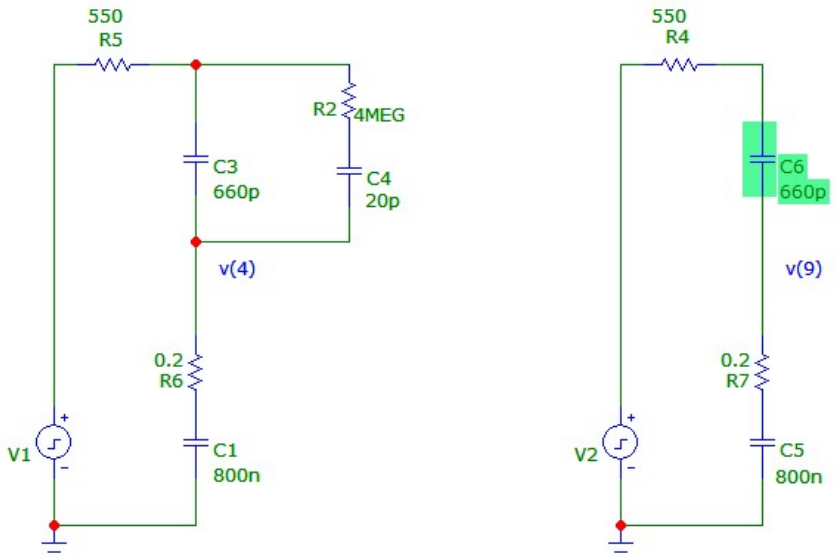

Figure 4.11. *Simulation circuit used to demonstrate "creeping".*

To simulate the creeping characteristics of the voltage divider the step response must be obtained. The step response of the divider before the added creeping compensation is shown in figure 4.12.

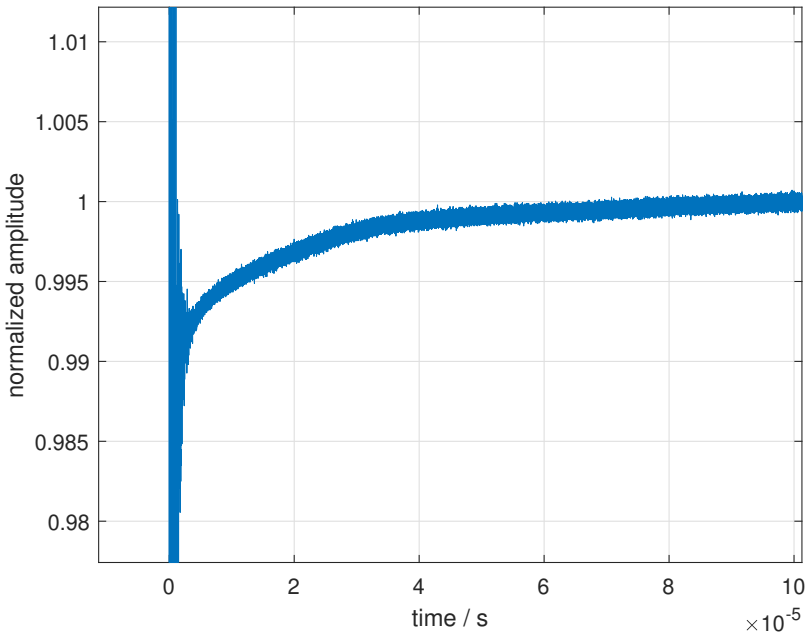

Figure 4.12. *Measured step response, zoomed to show a part of the creeping phenomenon.*

The creeping amplitude is 1 % and τ is 23 µs. These values might differ a bit from the reality since the step response has a lot of disturbance caused by the stray elements in the measurement equipment. Now all the values needed to calculate the compensation are known and presented in table 4.1.

Table 4.1. *The values used for calculating the compensation values.*

Element	Value
C_2	792 nF
τ	23 µs
$\frac{\Delta U}{U}$	1 %

Now using these values from table 4.1 and equation 2.10 the compensating branch in the low voltage arm should have capacitance of 7.9 nF and resistance of 2.9 kΩ. Because there are 4 branches in the low voltage arm it is beneficial to divide the compensation to each of the 4 branches i.e. dividing and multiplying the values by 4, respectively. Now the low voltage arm should have 4 similar compensation branches with values of 11.6 kΩ 1,98 nF in one branch. The chosen, nearest available, values were 10 kΩ and 1.8 nF.

The chosen components were of a through-hole-type and placed on top of the circuit board as shown in figure 4.14. The improvement of the compensation is shown in figure 4.13.

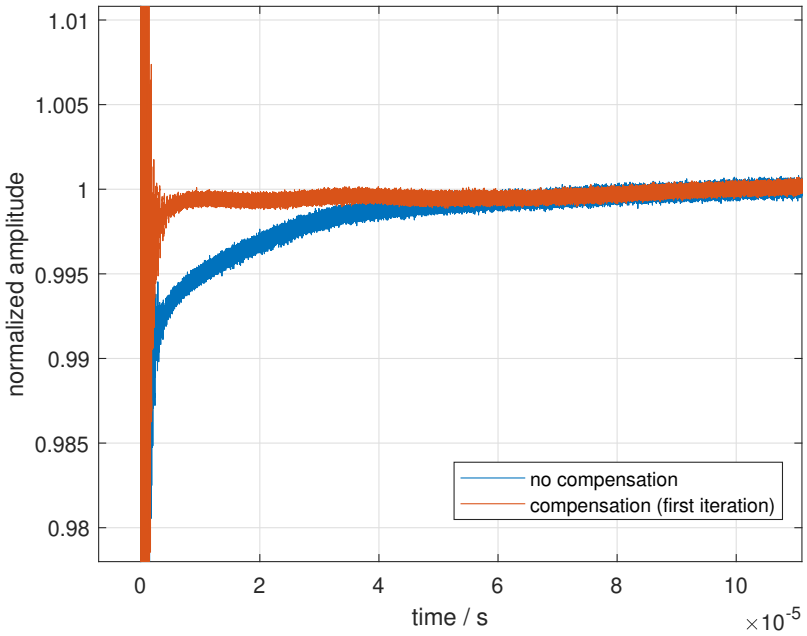

Figure 4.13. *Measured step response, zoomed to show how the creeping compensation improves the situation.*

The change is considerable when adding the compensation to the low voltage arm. Now there's smaller error in T_2 –the 50 µs mark– as can be observed from the step response. The step response still has some creeping but that is low compared to disturbances in the start of the response. The oscilloscope also may exhibit some non-ideal phenomena that is reflected to the measured waveform.

Figure 4.14. *PCB layout with compensation.*

Now that the compensation in the low voltage arm was done by measuring the creep of a signal that had been compromised with the creep of the measurement device as well as the actual creeping caused by the high voltage capacitors discussed in section 2.4 the compensation should be redesigned. Figure 4.20 shows how the compensation affected the system with and without step correction.

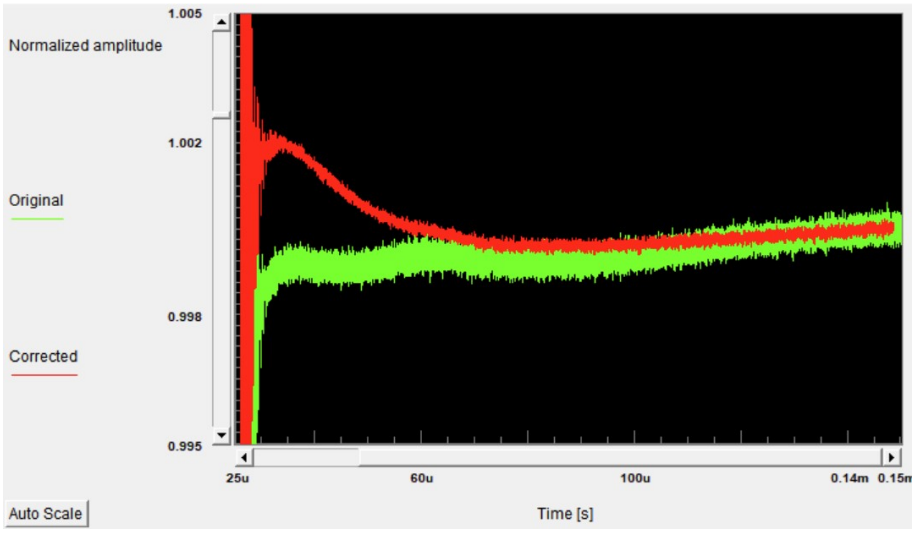

Figure 4.15. *The step correction program's results.*

After the first iteration of the component sizing according to fig. 4.13 waveform that had about 1 % of creeping amplitude was successfully compensated if the oscilloscope would act ideally. The oscilloscope in question is far from ideal as can be seen from figure

3.8. The response that appeared almost flat was in fact over-compensated, since the oscilloscope also had a bit of creeping. The resulting creeping is about 0.2 % after the first iteration. One notable thing is that the program seems to low-pass filter the results. This is because the convolution process is sensitive to noise and therefore needs additional filtering [30].

The compensation procedure was done again, but with a corrected waveform to measure the creeping parameters. The waveform is shown in figure 4.21.

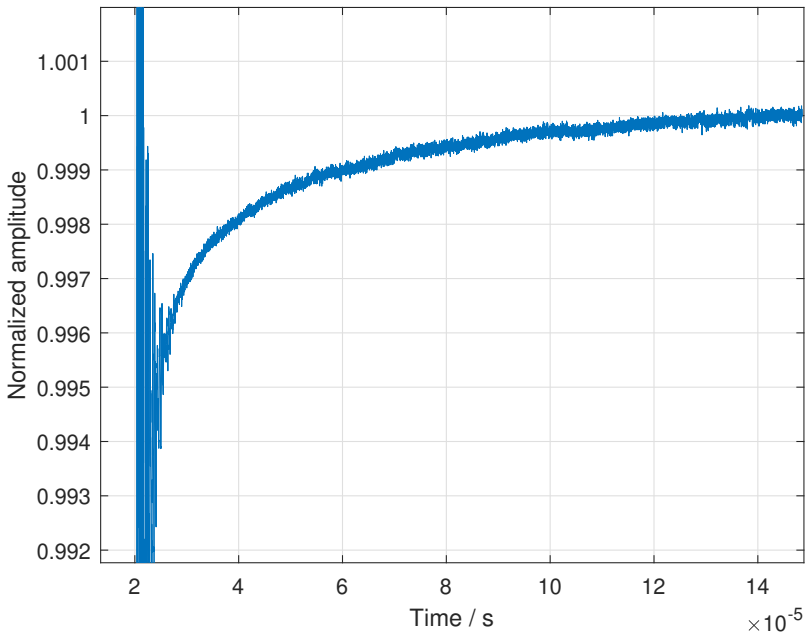

Figure 4.16. *Corrected step response and it's creeping characteristics.*

The creeping amplitude is now approximately 0.6 % and τ about 20 µs. These values when inserted to equation 2.10 give compensation parameters of ΔC_2 4.8 nF and ΔR_2 3.3 kΩ. This means that each of the 4 branches in the low voltage arm should have about 1.2 nF of capacitance and 13 kΩ of resistance in series.

The creeping amplitude can be easily determined so the capacitance value must be near optimal. Figure 4.22 shows how capacitance changes affect the compensation results. The 1.5 nF capacitors seem to be too large and 0.9 nF capacitors too small but still a bit better. So the optimal capacitor would be something in between these values.

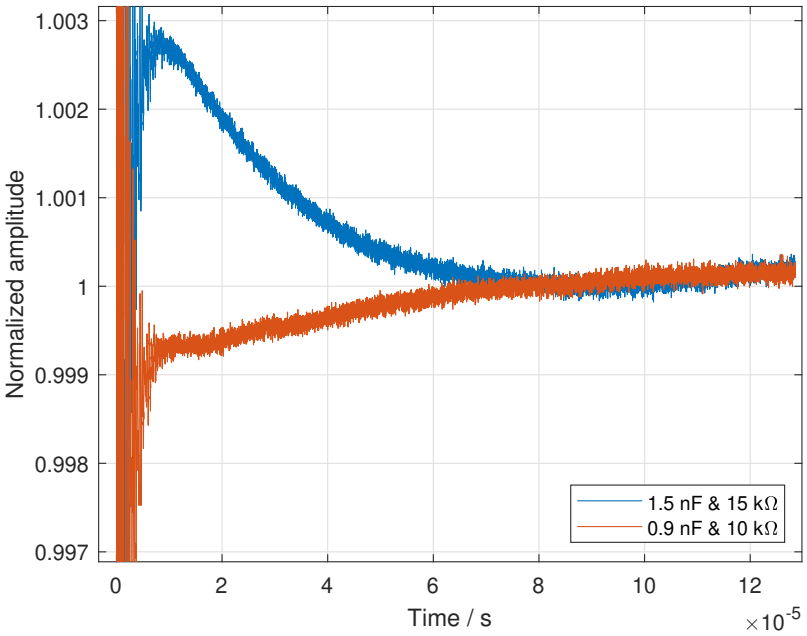

Figure 4.17. *Search of the correct capacitor values.*

The final chosen capacitance value was 1.1 nF. Then the resistance was altered and results plotted in figure 4.23. The 15 kΩ is the best value and the creeping characteristic stays inside ± 0.5 %. The final results is shown in figure 4.24.

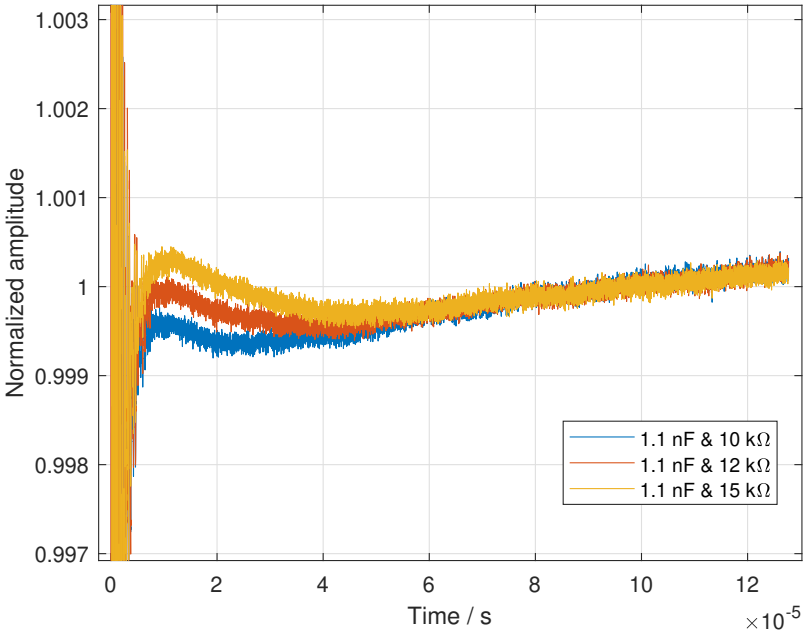

Figure 4.18. *Search of the correct resistance values.*

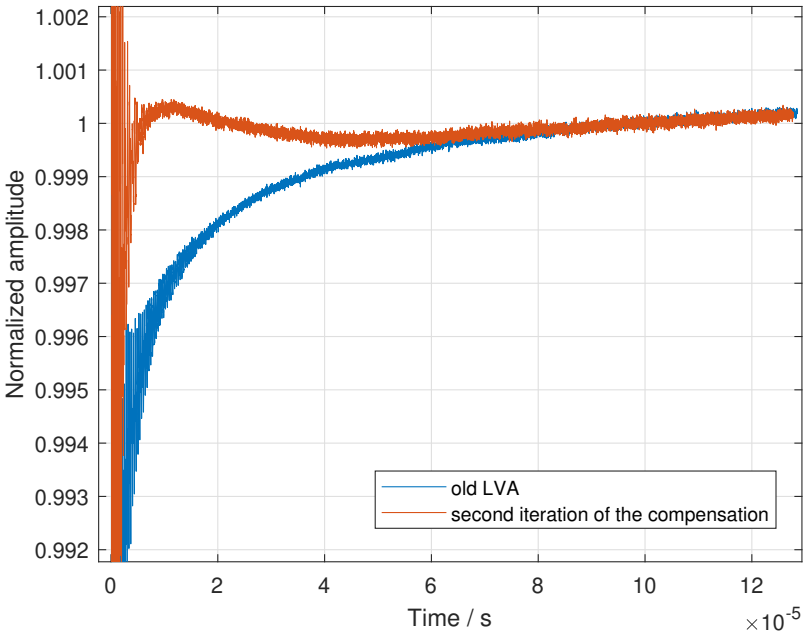

Figure 4.19. *Creeping characteristics with the old LVA made by a divider manufacturer and a new LVA with creeping compensation.*

The old low voltage arm has a lot of creeping since it has no compensation although the low voltage arm and high voltage capacitors are from the the same manufacturer. The figure shows also a different noise level. This is due to the convolution program [30]. The dynamic response is now significantly better, i.e. flatter.

4.2.2 Compensation with corrected oscilloscope response

The earlier described compensation was based on the creep measured directly with the oscilloscope without correcting the possible error of the oscilloscope. As it was later observed that the drift measurement error of the oscilloscope was actually rather notable, it was decided to re-design the compensation circuit based on the step response corrected oscilloscope data. Figure 4.20 shows how the compensation affected the system with and without step correction.

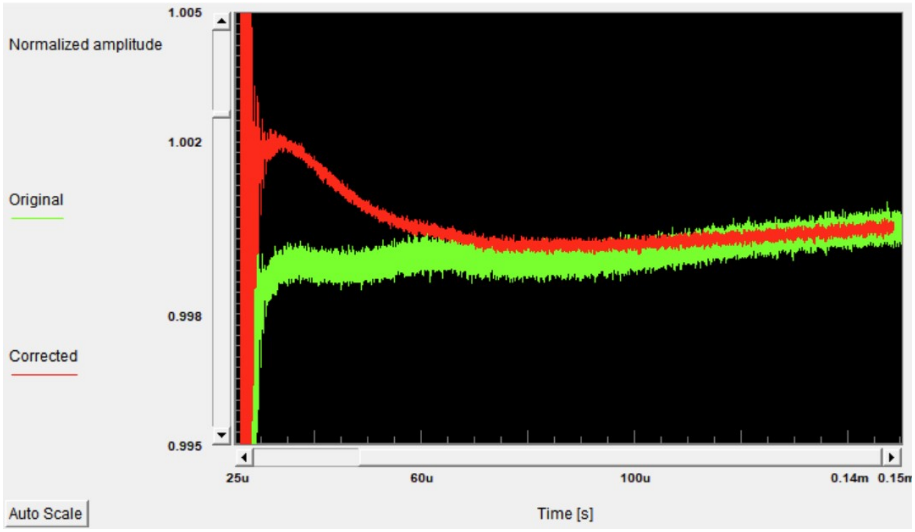

Figure 4.20. *Step correction program showing the real waveform and the waveform that the oscilloscope captures.*

So the first iteration of the component sizing according to fig. 4.13 waveform that had about 1 % of creeping amplitude was successfully compensated if the oscilloscope would have ideal performance. The oscilloscope in question is far from ideal as can be seen from figure 3.8. The response that appeared almost flat was in fact over-compensated, since the oscilloscope also had a bit of creeping. The resulting creeping is about 0.2 % after the first iteration. Another notable thing is that the program seems to low-pass filter the results. This is because the convolution process is sensitive to noise and therefore needs additional filtering [30].

The compensation procedure was done again, but with a corrected waveform to measure the creeping parameters. The waveform is shown in figure 4.21.

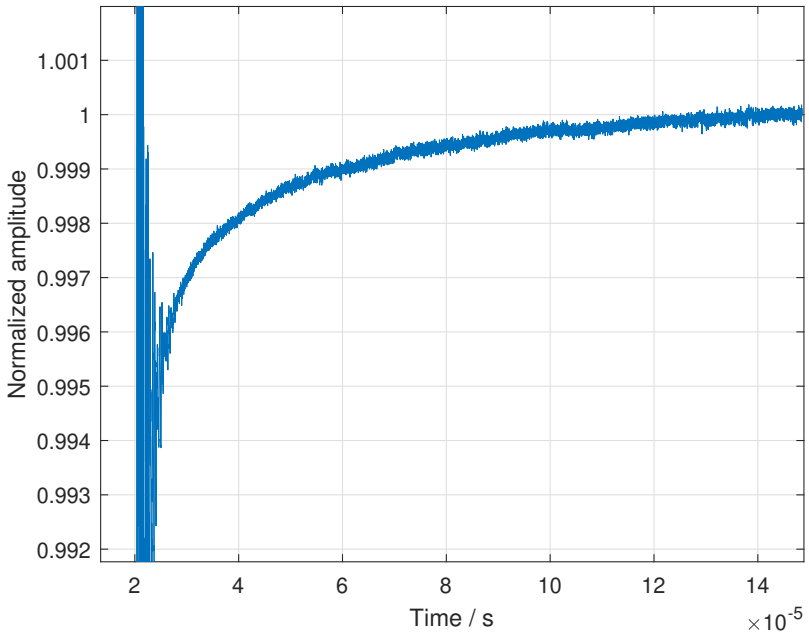

Figure 4.21. *Corrected step response and it's creeping characteristics.*

The creeping amplitude is now approximately 0.6 % and τ about 20 µs. These values when inserted to equation 2.10 give compensation parameters of ΔC_2 4.8 nF and ΔR_2 3.3 kΩ. This means that each of the 4 branches in the low voltage arm should have about 1.2 nF of capacitance and 13 kΩ of resistance in series.

The creeping amplitude can be easily determined so the capacitance value must be nearly optimal. Figure 4.22 shows how the capacitance changes affect the compensation results. The 1.5 nF capacitors seem to be too large and 0.9 nF capacitors too small but still a bit better. So the best capacitor would be something in between these values.

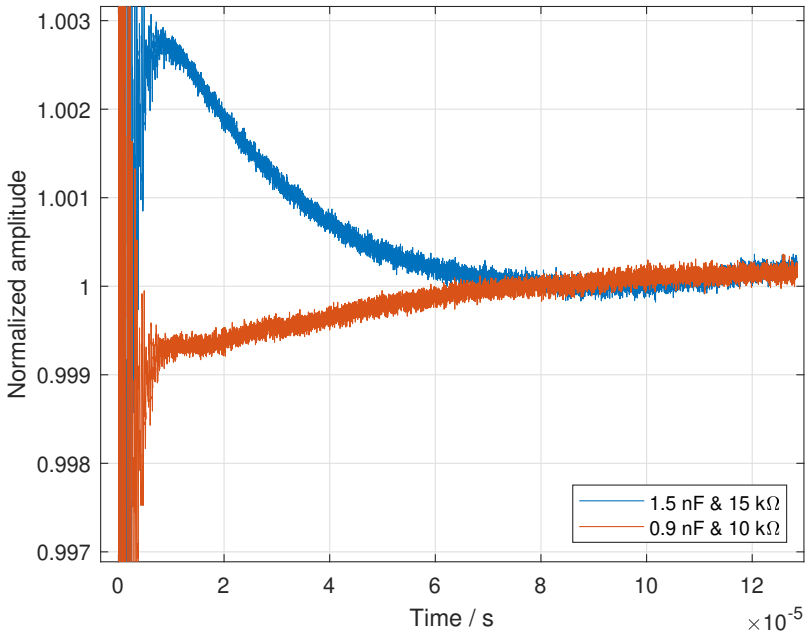

Figure 4.22. *Search of the correct capacitor values.*

The final chosen capacitance value was 1.1 nF. Then the resistance was altered and results plotted are in figure 4.23. The 15 kΩ was found to be the best value and the creeping characteristic stays inside ± 0.5 %. The final result is shown in figure 4.24.

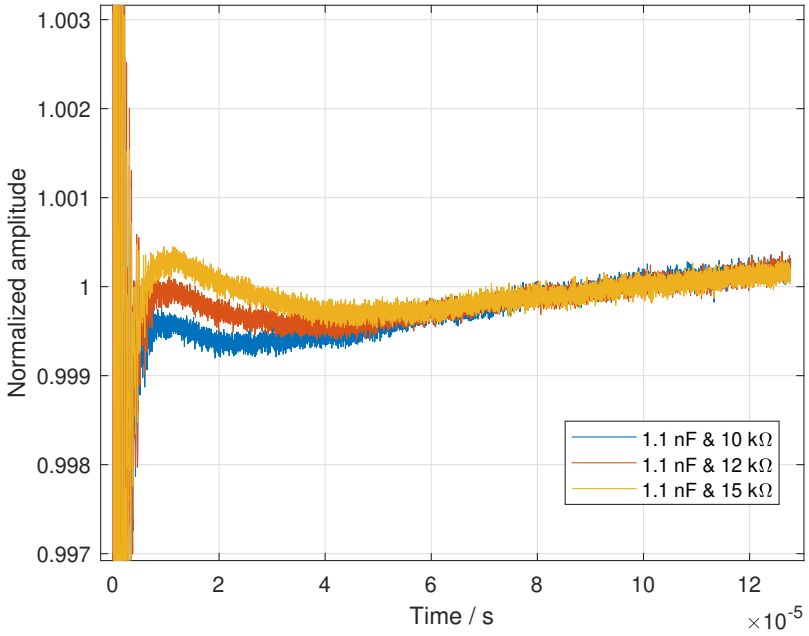

Figure 4.23. *Search of the correct resistance values.*

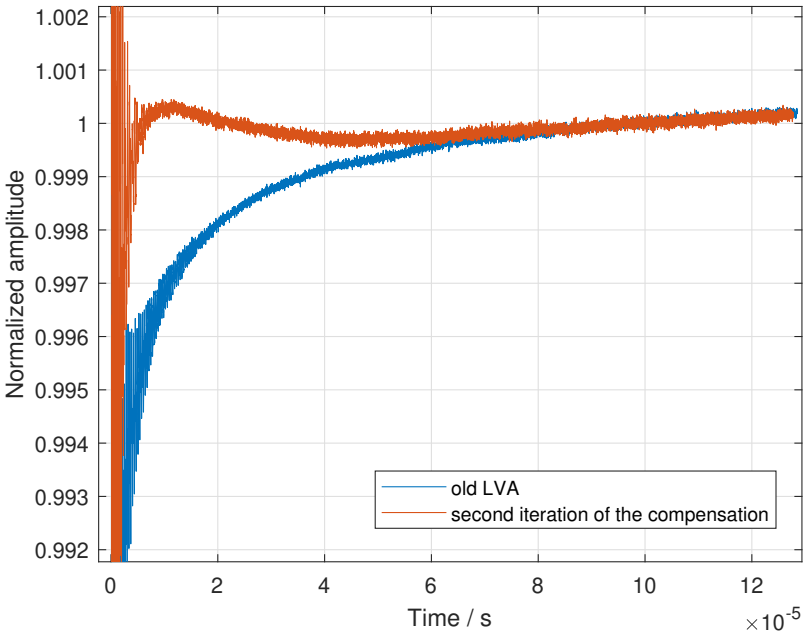

Figure 4.24. *Creeping characteristics with the old LVA made by the divider manufacturer and with the new LVA with creeping compensation.*

The old low voltage arm has a lot of creeping since it has no compensation although the low voltage arm and high voltage capacitors are from the the same manufacturer. The figure shows also a different noise level. This is due to the convolution program [30]. The dynamic response is now significantly better, i.e. the step response is flatter.

4.3 Inductance of the damping resistor

The inductance in the high voltage arm might cause some unwanted oscillations when the inductance forms an LC circuit with stray capacitances to ground. The high voltage capacitors may have significant inductance in them but that is hard to measure since the capacitor is mostly capacitive.

The bifilarly wound damping resistor can be measured more easily with an LCR meter. The results from the inductance measurement are gathered to the table 4.2. The measurement was taken with series measurement mode and additional measurement leads.

Table 4.2. *Inductance of the damping resistor measured with an LCR-meter.*

Quantity / Frequency	1 kHz	10 kHz	100 kHz	1 MHz
L (µH)	5.7	6.9	7.3	7.7

The damping resistor has significant inductance and that combined with the inductance inside the capacitors results in even higher inductance in the HVA. The measured in-

ductance gets higher as the measurement frequency increases. This might be due to measurement setup's unidealities like stray capacitances or extra measurement leads having stray capacitance and self inductance although the open circuit trim should work quite well.

To investigate, if the situation regarding the oscillations in the front could be mitigated by ordering a better damping resistor, a study was performed with through-hole resistors with low inductivity. The resistors used were of a carbon film type resistors that have much lower inductance value, even when added in series to gain the same resistance value than the damping resistor has.

Another concern regarding the damping resistor is that the damping resistor is not dispersed along the HV column. Almost all of the damping resistance lies at the top of the capacitor stack. Ideally, the damping resistor should be divided along the HV column while one big part of it still remaining at the top. This would reduce the oscillations caused by the inductance and capacitance of the circuit.

The 230 Ω resistance at the top was replaced by 180 Ω resistance and 2 resistance of 33 Ω inbetween the 3 capacitors as shown in figure 4.25. The capacitors are connected together via intermediate connection blocks. These blocks allow the insertion of the resistances because the bottom contact to the intermediate connection block is done only via bolts' threads and through the bolts themselves. So the bolt can be insulated or changed to a insulating threaded rod material. This however only works on low voltage step testing so if this method improves the situation, more detailed construction need to be build to house the even bigger resistors and to provide insulation so no breakdown discharge occurs.

The intermediate resistances would damp the oscillating LC circuit that is formed by the HVA inductance and stray capacitance to ground. The figure 4.26 shows how the situation alters the step response.

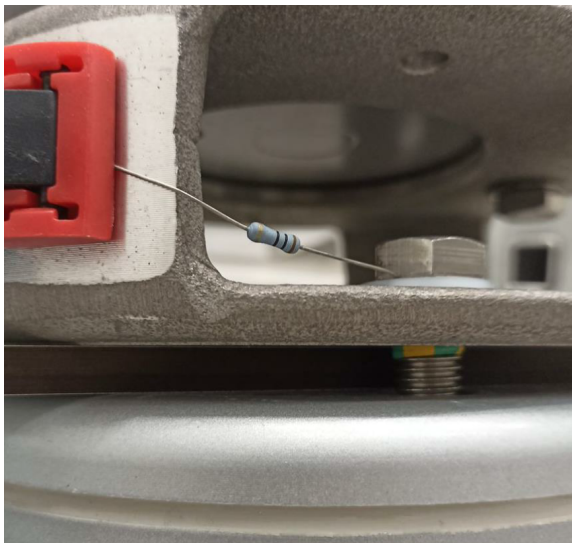

Figure 4.25. *Setup for the distribution of the damping resistance.*

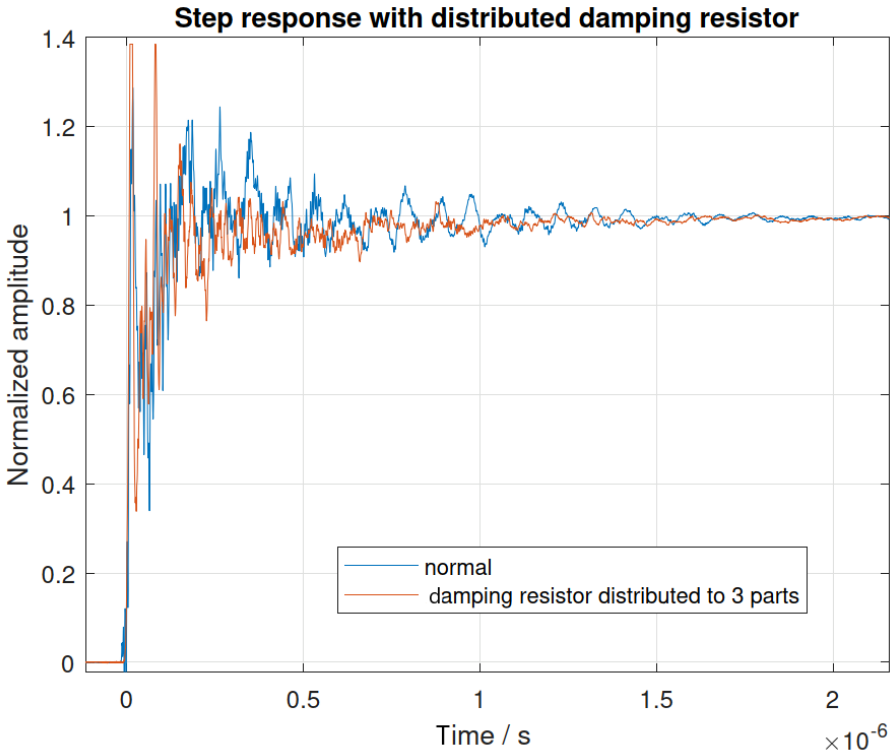

Figure 4.26. *Effect of damping resistor distributed to 3 parts.*

As can be seen, the oscillatory behavior still remains. The situation is slightly better at around 0.5 µs. The step response also is a bit slower but this is due to the new low inductive HVA damping resistance being higher. This results in slightly different resistive and capacitive scale factor which alters the response. This however may be ignored since the interest is in the oscillatory behavior.

5. UNCERTAINTY ANALYSIS

Uncertainty analysis needs different input uncertainty components. These are the calibrating system's uncertainty and the uncertainty due to the long term drift of the scale factor for example. The necessary uncertainty contributions are determined experimentally, and if not possible, approximated. The high voltage arm is the same for all of the different setups studied so some of the standard uncertainty contributions are the same for both systems like the proximity effect.

5.1 Temperature effect

When the temperature of the divider changes, so will the insulating materials' characteristics as well as dimensions of metal materials for example. This results in a change of the capacitance values. If the high voltage capacitances change, so will the scale factor also. The LVA capacitors' temperature dependency can be read from the data sheet.

The HV capacitors don't have a data sheet so measurements are taken. The instrument to measure the capacitance is a LCR meter LCR-8101G by GW-Instek. The measurements are carried out in a climate room that has controllable temperature and humidity conditions. The setup is shown in figure 5.1.

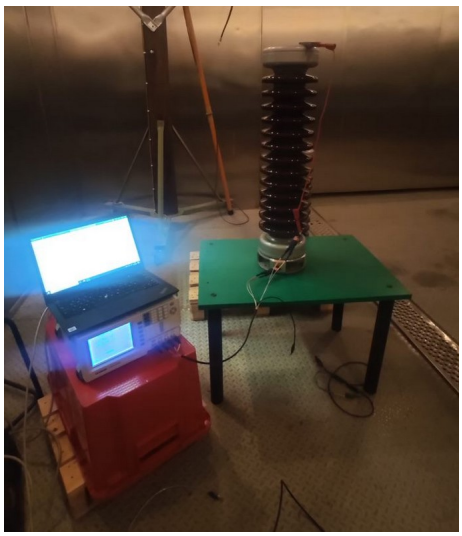

Figure 5.1. *Setup for temperature tests.*

The LCR meter has additional cabling because the HV capacitor units are too long for the normal LCR meter cables. The additional wire has self inductance and capacitance and that will interfere with the reading. The solution to overcome this is to use a built-in trim function that measures the open circuit capacitance and saves it and while doing actual measurements, the program subtracts that stray capacitance from the actual capacitance of the device under test. The cabling was tried to be kept in approximately in similar location during the measurements since a change in position of the additional cable would impact the measurement system properties which would affect the measured value.

The LCR meter was used with 2 V_{AC}. The series capacitance and resistance were measured with different frequencies for the AC voltage. The results are expressed in figure 5.2 for the 1 kHz, 2 V_{AC}, measurement mode.

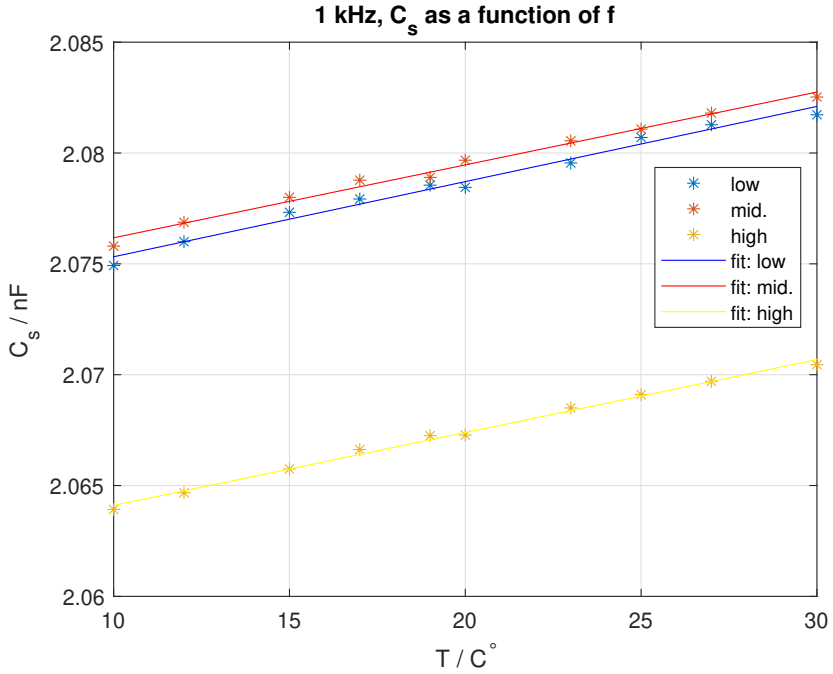

Figure 5.2. *Results for temperature tests.*

All the HV capacitors have the same slope, as expected. The offset for the highest capacitor is a bit lower so it might be from a different production batch. This isn't an issue since the slope is the most important for assessing uncertainties due to temperature effects.

The fit line for the lowest capacitor

$$C\left(T\right) = 2.072 + 0.0003391T \ [\mathrm{nF}], \tag{5.1}$$

where T is the temperature of the divider. If the temperature increases by 10 degrees Celsius, the lowest capacitor value will increase by 3.4 pF which is about 1700 ppm.

For example when 19$\pm$2 ºC is considered as the calibration temperature, meaning that

the temperature of the lab is 19 ºC and the temperature changes as maximum to 21 ºC or as minimum to 17 ºC, the uncertainty can be calculated for u_{B5} by equation 2.32. The worst case is when the temperature changes to the maximum or minimum. The HVA capacitors have a positive temperature coefficient but the low voltage arm capacitors' datasheet only states the coefficient by ± 30 ppm so the sign is unknown. The negative coefficient results in larger u_{B5} so that needs to be used to be on the safe side. For ± 2 ºC of variance in the lab temperature results in u_{B5} being 0.00021929.

5.2 Proximity effect

The proximity effect to the overall uncertainty needs to be determined for the uncertainty evaluation. As stated in equation 2.32 the worst cases for the scale factor are used to determine u_{B6}. The proximity effect affects the scale factor of the system due to neighboring grounded or energized objects via stray capacitances. The worst cases are therefore with highest stray capacitance i.e. when the divider is at the closest to a grounded, or energized, object like the laboratory's wall.

Figure 5.3 presents how the distance to neighboring objects is measured and how the test setup looks like. The aluminium door is grounded with extra grounding to provide better grounding conditions as well as protect the door control mechanism if a flash-over occurs. The measured distance is taken from the divider midsection to the nearest point of the door. The distance to the generator is taken similarly but the end point is in the middle of the two support beams.

Figure 5.3. *Test setup for measuring the proximity effect.*

The divider is stressed with standard front time LI voltage from the generator while altering the distance. The voltage level is +200 kV and 5 stages of the generator are used. Ten pulses are performed for each of the distance points and the average taken from those. The results are expressed in figure 5.4. The zero point is approximately in the middle, in between the generator and the door, which is roughly the normal position the divider is located in most of the measurements.

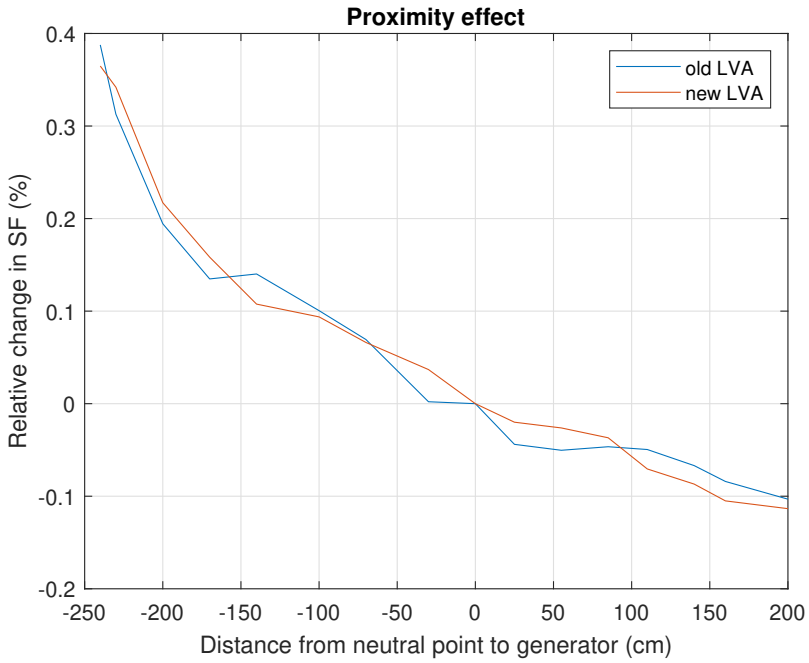

Figure 5.4. *Results for the proximity effect.*

The charging voltage of the generator is kept the same and only the position of the divider is changed, while keeping the connecting lead in approximately similar angle and position. The final positions are both about 1 m away from the studied neighboring object. The voltage fed to the divider is the same but the measured voltage decreases when moving towards the wall. This means that the scale factor increases as well the same amount, relatively. The figure 5.4 shows also that both of the low voltage parts behave similarly and the most severe case is the one with a grounded object.

The results are very similar for both of the low voltage arms because of that stray capacitive coupling connects mainly to the high voltage arm, which is the same in both systems. The scale factors are approximately the same so the effect scales to the recorded waveform similarly. The figures 5.5 and 5.6 show the proximity effect for the wall and generator separately.

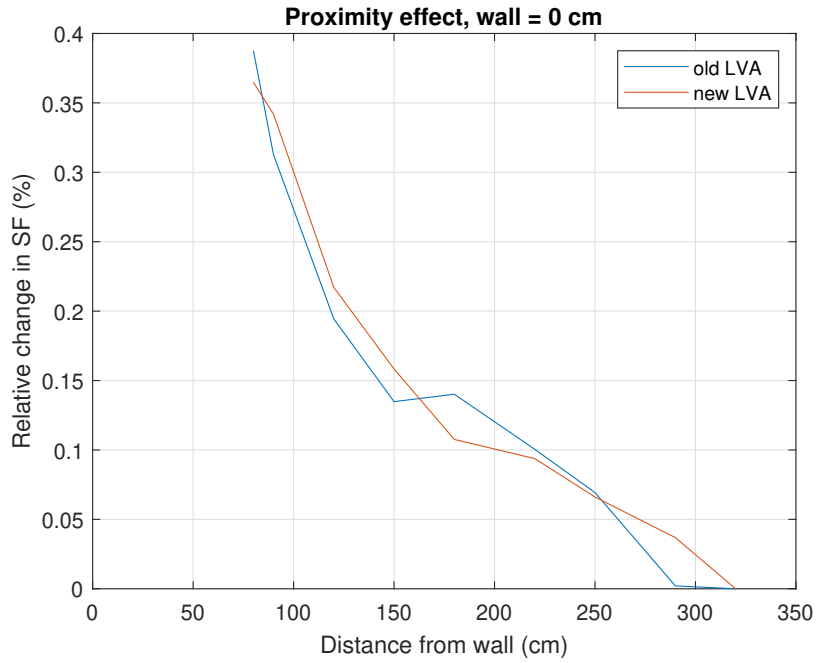

Figure 5.5. *Results for the proximity effect (wall only).*

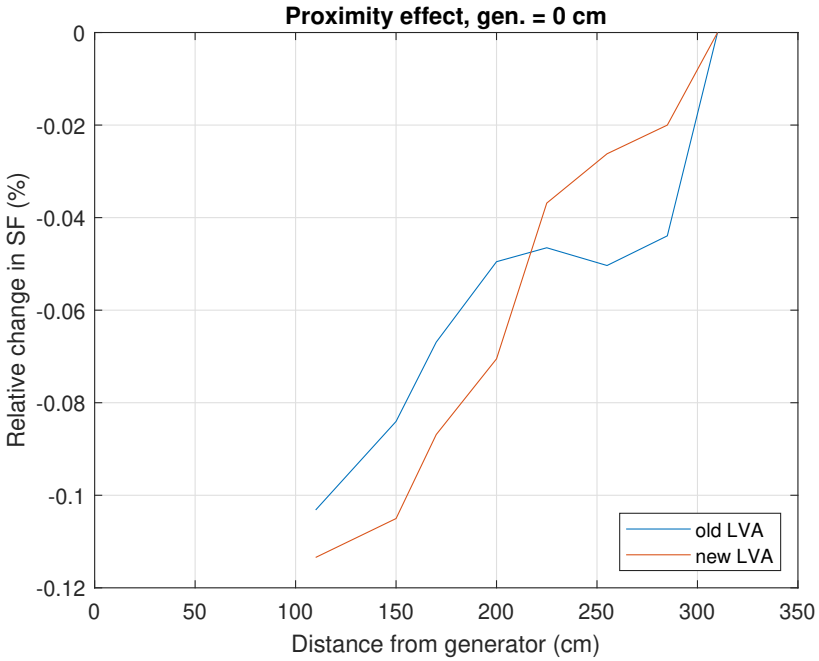

Figure 5.6. *Results for the proximity effect (generator only).*

The figures have a wide location range studied. It should be noted that the divider will never be used f.ex. less than one meter from the wall. In practice the divider is used as far from wall and generator as possible and this of course depends on the measurement setup used.

The results for u_{B6} can be set for different ranges. The latter uncertainties are the worst

cases, the divider is rarely less than one meter from the grounded wall. To find a uncertainty contribution relevant to the divider position inside the laboratory.

Table 5.1. *Uncertainties u_{B6} for different clearances.*

Distance from wall and generator (both)	u_{B2}% old	u_{B2} % new
>150 cm	0.1574	0.1683
>200 cm	0.1097	0.1173
>250 cm	0.0620	0.0663
>300 cm	0.0143	0.0153

As can be seen from the table 5.1, the uncertainty contribution gets higher when the divider is more near to the grounded or energized objects. Both the old and new LVAs behave similarly with almost no difference. The divider will always be 2 meters or more away from the wall or LI generator so the resulting standard uncertainty contribution u_{B6} will be 0.11 % for both of the new and old system.

5.3 Non-linearity effect

The reference divider can measure maximum of 400 kV LI. The divider under analysis is a 1 MV divider so the additional linearity tests should be performed.

The linearity was tested by measuring the LI with the divider and simultaneously measuring the impulse generator's DC charging voltage with a DC measurement system. The test voltage waveform was captured with the measurement system under calibration. The charging voltage of the impulse generator was measured with a 200 kV voltage divider and a multimeter.

For the old system the calibration certificate M-19E220 shows the linearity test results. The additional linearity was calculated by measuring two voltage levels, one of which was out of the range since the measurements were performed for over 5 voltage levels. The deviation from the mean of the ratio was 0.04 % and the standard deviation 0.05 %. The estimated uncertainty results in 0.7 % with a confidence level of 95 % (k = 2). The linearity effect should be the same for the new system because the high voltage arm is the same.

5.4 Dynamic behaviour

Dynamic behaviour uncertainty contribution can be estimated with a measurement of the divider's step response with the upper and lower limit of the nominal epoch. This means that the front time should be varied from the nominal 1.2 µs to $\pm$ 30 %. The front time therefore needs to be set to 0.84 and 1.56 µs also when firing pulses to the divider.

The appendix A shows the calibrations for the divider. The scale factor of 1157.7 is used which is calculated by using the components' values. That is about 3 % off from the scale factor that is measured.

From the results the dynamic behavior can be obtained. The short and long front results for the parameters vary a lot from the standard front pulse. The standard uncertainty related to dynamic behavior for the scale factor is presented in table 5.2. The u_{B2} value is calculated from appendix A using the equation 2.27. For the old system, the calibration certificate M19E220 is used.

Table 5.2. *Uncertainties u_{B2} for the three different systems.*

System	u_{B2} (%) U_{peak}	u_{B2} (%) T_1	u_{B2} (%) T_2
Old system	0.3168	0.4010	0.7391
New system with DIAS® 733	0.1466	1.435	0.1362
New system with NI	0.2030	1.041	0.1936

The new system has a lot larger dynamic effect on the measured waveform. This is because it has a lot faster but also more oscillatory response. The most notable is the uncertainty difference in T_1 between the NI and DIAS® 733. This is due to the correction made to the NI digitizer. The uncertainty of T_2 is much better in the new system.

5.5 Short-term stability

The short term stability needs measurement of the scale factor before and right after it has been in use. This can be done by measuring the HVA with an LCR-meter before firing 10 pulses to the divider with full operating voltage. After the pulses have been fed, the divider's capacitance should be measured again and the short-term stability contribution estimated from those measurements. This effect is mainly caused by heating of the components during testing so the divider's temperature will be a bit higher than the laboratory's air temperature at the end of the measurements.

The most demanding part when measuring this effect is the time. The grounding should be done quickly after the last pulse and measurement done after that. This may be challenging when considering the safety of the measuring personnel. After the grounding has been made the measurement setup for the HVA needs to be built. This takes time and while building the setup the divider may cool down too much. The heating of the divider is more prominent in resistive dividers. The standard uncertainty component for short term stability is estimated to be 0.07 %.

5.6 Long-term stability

For the newer system, the long-term stability of the scale factor can be evaluated from two consecutive calibrations with a type B uncertainty or by multiple calibration checks with a type A uncertainty, the latter however needs a lot of data to be a good evaluation method. The type B uncertainty for the long-term effect for the old system was calculated from two calibration checks.

The table 5.3 combines the results from the calibration history. The scale factor has been the same 700.2:1 the whole time so the errors can be combined to the table and using them, calculating the long term drift of the system.

Table 5.3. *Scale factor determinations from different calibration times.*

Old system calibration year	mean error % of the SF (standard front)	SF corrected
2010	-0.44	703.3
2013	-0.22	701.7
2016	0.44	697.2
2019	0.17	699.0
2020	-0.1	700.9

From the results in table 5.3 the long-term stability contribution can be calculated using the equation 2.29. The results are presented in table 5.4.

Table 5.4. *Type B uncertainties u_{B4} for the three different systems.*

Calibration years compared	u_{B4} (%)
2010 – 2013	0.13
2013 – 2016	0.38
2016 – 2019	0.16
2019 – 2020	0.47

The long term results deviate from each other a bit. This might be partly due to the changes in the reference system over the years. The oldest calibrations that date back to 2010 had different reference system. The HUT-400 divider is the same but the transient recorder has been changed to a new one and the software of the transient recorder is also continuously updated. The latest version of the recorder has uncertainties (k=2) stated to be 0.1, 1 and 0.5 % for U_p, T_1 and T_2, respectively. That also explains why the scale factor drift changes also direction. The u_{B4} stays below 0.5 %. The 2019–2020 entry value is so high because the calibrations are done 3 years apart and the time of use is set to 3 years which is the normal calibration interval. This means that the latter part of the formula 2.29 gets larger.

Since there are many calibrations available the type A uncertainty can also be calculated. The resulting u_{B4} by using equation 2.30 is 0.41 %. The standard [4] doesn't specify how many calibrations are needed to be available for type A uncertainty to be valid to use.

To be on the safe side, the largest u_{B4} needs to be used. The type A evaluation might not be the most accurate since there are only 5 certificates used to calculate it and the digitizer of the reference system has been changing over the years. The largest uncertainty contribution is 0.47 %. This can be used for the new divider also since drift of the scale factor is mainly due to the aging of the high voltage arm components.

5.7 Software

VTT's digitizer's uncertainty contribution u_{B7} is given in the record of performance for LIVeval4 software. The uncertainties for front time, tail time and peak value are 0.35, 0.05 and 0.02 % respectively.

The uncertainty contribution for the DIAS 733 digitizer that is a part of the TAU's system is expressed in the datasheet made by the manufacturer. The peak voltage uncertainty is stated to be 1 % and for the time parameters the uncertainty is 2 % which is the expanded uncertainty. [26] All the uncertainties are collected to the table 5.5.

Table 5.5. *Uncertainties u_{B7} for different setups.*

System	u_{B7} for U_{peak} (%)	u_{B7} for T_1	u_{B7} for T_2 (%)
DIAS 733	0.5	1	1
VTT's digitizer	0.02	0.35	0.05

5.8 Type A uncertainty

For the type A uncertainty for the time parameters as well as the peak value are calculated by the maximum standard deviation of all the voltage levels recorded and dividing the value by the number of pulses performed for each voltage level. The result is the u_A standard uncertainty.

For the first calibration, the uncertainties are presented in table 5.6.

Table 5.6. *Uncertainties u_A for different setups.*

System	u_{B7} for U_{peak} (%)	u_{B7} for T_1	u_{B7} for T_2 (%)
DIAS 733	0.0168	0.174	0.0288
VTT's digitizer	0.00962	0.121	0.0133

The uncertainties are quite similar for the two new systems. The peak value and the tail time have much lower type A uncertainty than the front time. This is because of the dynamic behavior in the divider that the step response shows. Also the NI system has better u_A than DIAS®733. For example the 0.02 % uncertainty of the front time of the DIAS (new system) is about 0.2 in terms of the scale factor, which is quite small considering that the scale factor is in the magnitude of 1100:1. When considering the front time the 0.174 % uncertainty results about 3 ns of uncertainty in a standard 1.2 µs T_1.

The B type uncertainty contribution u_{B0} is calculated from the largest deviation of the mean of all the voltage levels used. A figure 5.7 shows how the scale factor changes when voltage level changes.

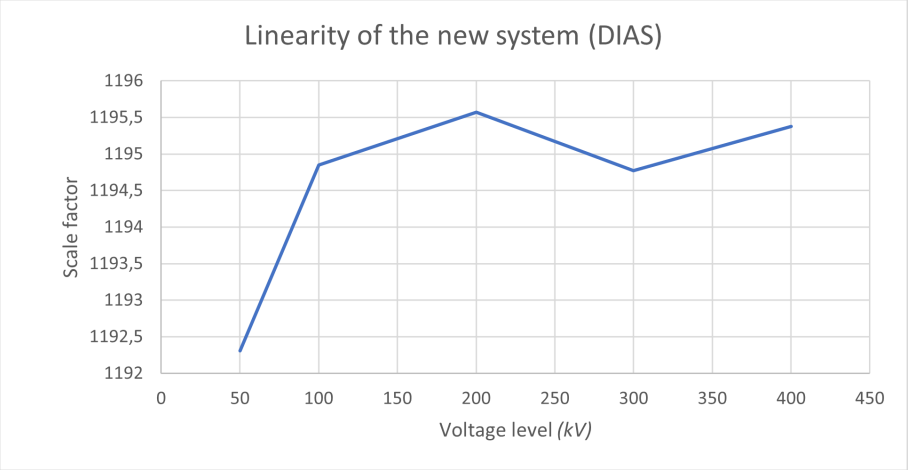

Figure 5.7. *Linearity of the scale factor over the calibration range of voltages for the new system with DIAS digitizer.*

The change in the scale factor over the calibration range is treated as a type B uncertainty so the largest deviation from the mean is taken and divided with $\sqrt{3}$. The results for u_{B0} for the DIAS system is 0.16 % and for the NI system 0.23 %. This is the uncertainty contribution caused by the deviations inside the calibrating system's range. This however covers only the calibration range. To extend the uncertainty to cover the whole system capability, additional linearity test with f.ex. a sphere gap should be performed if the reference system cannot be used for the whole range of the device under calibration.

When using the reference method to calculate the expanded uncertainty this type A uncertainty isn't needed. The uncertainty is calculated from the uncertainty of the reference system and adding the type B contributions for the system under study f.ex. the temperature dependency effect.

5.9 Expanded uncertainty & uncertainty budget

The individual, uncorrelated, uncertainty contributions are summed together by the equation 2.34 the coverage probability results in approximately 68 % confidence interval if all the contributions are uncorrelated. To obtain 95 % confidence level, the value is multiplied with *k* = 2.

The expanded uncertainty calculation needs also the uncertainty of the reference system. The used reference system has uncertainties ($k = 2$) stated to be 0.5 %, 2 % and 1 % for the peak voltage, front time and time to half value, respectively.

The old system's uncertainties are assumed to be the same as in the new system with DIAS digitizer excluding the dynamic component which is calculated from previous calibration certificate to be 0.23, 1.22 and 1.04 % for the peak value, T_1 and T_2, respectively. The resulting expanded uncertainty is 1.7, 3.1 and 3.1 % of the peak value, T_1 and T_2 respectively for the old system.

The uncertainties of the peak value parameter are presented in table 5.7. The time parameter uncertainties are gathered to table 5.8.

Table 5.7. *Uncertainty evaluation of the peak value for the new system.*

	DIAS U_T(%)	NI U_p(%)
u_{ref}	0.25	0.25
u_{B1}	0.35	0.35
u_{B2}	0.15	0.20
u_{B3}	0.07	0.07
u_{B4}	0.47	0.47
u_{B5}	0.02	0.02
u_{B6}	0.11	0.11
u_{B7}	0.5	0.05
$U_{k=2}$	1.7	1.4

All the expanded uncertainties of the three studied systems are gathered in table 5.9.

As can be seen, the new system has better T_2 and U_{peak} uncertainties. The T_1 uncertainty is worse with DIAS and approximately the same with NI when compared to the old system. This is because of the oscillatory step response the divider has that results in large deviations when firing pulses with slow and fast front times.

The effect of the compensation can be seen from the improvement of the tail time. The new system with DIAS has still relatively large uncertainty which is mainly due to the

Table 5.8. *Uncertainty evaluation of time parameters for the new system.*

	DIAS T_1(%)	NI T_1(%)	DIAS T_2(%)	NI T_2(%)
u_{ref}	1	1	0.5	0.5
u_{B2}	1.51	1.10	0.15	0.21
u_{B7}	1	0.5	1	0.25
$U_{k=2}$	4.2	3.2	2.3	1.2

Table 5.9. *Uncertainties of the three studied systems.*

	U_{peak}(%)	U_{T1}(%)	U_{T2}(%)
Old system	1.7	3.1	3.1
New with DIAS	1.7	4.2	2.3
New with NI	1.4	3.2	1.2

digitizer and not the compensation itself. Also one reason the T_2 has still about one percent of uncertainty is due to the frequency dependency not following exactly first order response.

6. CONCLUSIONS AND FUTURE WORK

This thesis concentrated on studying lightning impulse measurements. The objective was to improve the existing system by designing and implementing a new low voltage arm and a measurement cable and later to do uncertainty analysis and calibration for the system. The old system showed significant creeping characteristics in its step response and it was substantially slow.

The new system introduced a new measurement cable as well as a new low voltage arm. The new low voltage arm was designed to fit additional circuitry to compensate for the frequency dependency caused by the high voltage arm. The step response showed about 1 % of creeping which resulted in relatively large error in T_2 parameter. The creeping phenomenon, caused by the high voltage arm, followed closely a 1st order response. The compensation was added to the new low voltage arm to match the amplitude and time constant by adding a RC circuits parallel to the low voltage capacitors. The resulting step response was improved and the creeping was kept under $\pm$ 0.1 %.

Smaller dimensions and printed circuit board elements replaced the old through hole type components to achieve less inductive low voltage arm. The resulting low voltage arm was significantly faster. This resulted in more oscillatory behavior, which was problematic in regards to the front time evaluation. The oscillation causes were investigated but no solution to damp the oscillations was found.

The main problem with the new system and its voltage divider is the high voltage arm. The damping resistance is not divided along the divider column as it ideally should be but is only placed on top of the high voltage capacitors. This together with the unidealities of the capacitors and decreased inductance of the low voltage arm results in high oscillations when the divider is fed with fast transients. The oscillations on the front result in high uncertainties for the front time.

The expanded uncertainties of both the original measuring system and the new system fulfill the requirements of reference measuring system (1 % and 5 % for the peak and time parameters, respectively [4]). However, although the uncertainty of T2 was improved with the new LV arm, the high frequency oscillations resulted in increased uncertainty of T1 parameter since the shape of the pulse has a large effect on the measurements.

The current damped capacitive divider of Tampere University was found to be in fact a

capacitive divider with added damping resistor at the top. The old system was designed so that it was slower and would thus "hide" the unideal behavior caused by the high voltage arm. When adding a new, faster, low voltage arm, the unidealities start to affect the measurements. The old system is functional as a laboratory's measurement system. The improved system can't be used as a reference system because of its high voltage arm.

The system could be further improved by ordering a new high voltage arm with more ideally behaving capacitors as well as more distributed damping resistor. The availability and investment aspects regarding this is rather troublesome so it will not be covered in this thesis.

REFERENCES

[1] Nousiainen, K., Elovaara, J., Karttunen, M., Aro, M. and Palva, V. *Suurjännitetekniikka*. Helsinki: Otatieto, 2015. 537 p. ISBN: 978-951-672-375-7.

[2] Hauschild, W. and Lemke, E. *High-Voltage Test and Measuring Techniques*. 2nd ed. 2019. Springer International Publishing AG, 2018. ISBN: 9783319974590.

[3] Kind, D. and Feser, K. *High-voltage test techniques*. 2nd ed. Oxford: Newnes, 2001. ISBN: 0-08-050810-3.

[4] International Electrotechnical Commission IEC. *International standard IEC 60060-1:2010 – High-voltage test techniques – Part 1: General definitions and test requirements*. Version 3. Geneva - Switzerland, 2010.

[5] Kuffel, J. and Kuffel, E. *High Voltage Engineering Fundamentals*. Oxford: Elsevier Science and Technology, 2000. ISBN: 9780750636346.

[6] Schon, K. *High Impulse Voltage and Current Measurement Techniques Fundamentals – Measuring Instruments – Measuring Methods*. 1st ed. 2013. Springer International Publishing, 2013. ISBN: 3-319-00378-X.

[7] Berlijn, S. Influence of lightning impulses to insulating systems - PhD thesis - Technische Universität Graz. PhD thesis. May 2000.

[8] Bergman, A. and Hällström, J. Impulse dividers for dummies. *Proc. Int. Symp. High Voltage Eng. (ISH)* (2003), pp. 1–4.

[9] Passon, S. *Experimentelle Untersuchung eines breitbandigen ohmsch-kapazitiven Teilers zur Messung von Gleichspannungen bis 600 kV*. ger. Technische Universität Braunschweig - Faculty of Elektrotechnik, 2017.

[10] Klüss, J. *Lecture notes in High Voltage Engineering*. Sept. 2013. URL: https://noppa.aalto.fi/noppa/kurssi/s-18.3150.

[11] Kreuger, F. H. *Industrial High Voltage: 4. Coordinating, 5. Testing, 6. Measuring*. 1st edition. Netherlands: Delft University Press, 1992, pp. 59–71. ISBN: 90-6275-562-3.

[12] McNally, J. R. M. *Non-inductive wire wound resistors*. U.S. Patent 2 937 355, May. 1960. URL: https://patents.google.com/patent/US2937355.

[13] Campisi, F., Rinaldi, E., Rizzi, G. and Valagussa, C. A new wirewound resistive divider for steep front impulse tests: design criteria and calibration procedure. *1999 Eleventh International Symposium on High Voltage Engineering*. Vol. 1. 1999, 164–167 vol.1. DOI: 10.1049/cp:19990533.

[14] Altgilbers, L. L. *Explosive pulsed power*. London, 2011. URL: https://andor.tuni.fi/permalink/358FIN_TAMPO/1j3mh4m/alma9910662049005973.

[15] Li, Y. and Rungis, J. Compensation of step response "creeping" of a damped capacitor divider for switching impulses. *11th International Symposium on High-Voltage Engineering (ISH 99)*. London: IEE, 1999, 1.128.P4–1.131.P4. ISBN: 0852967195.

[16] Coleman, H. W. *Experimentation, validation, and uncertainty analysis for engineers*. Hoboken, NJ, USA, 2018. URL: https://andor.tuni.fi/permalink/358FIN_TAMPO/1j3mh4m/alma9911130694705973.

[17] International Electrotechnical Commission IEC. *International standard IEC 60060-2:2010 – High-voltage test techniques – Part 2: Measuring systems*. Version 3. Geneva - Switzerland, 2010.

[18] Guides in Metrology, J. C. for. *JCGM 100: Evaluation of Measurement Data - Guide to the Expression of Uncertainty in Measurement*. Tech. rep. Accessed: 15.12.2021. JCGM, 2008. URL: https://www.bipm.org/en/publications/guides.

[19] Silva, F. F. da. *Electromagnetic Transients in Power Cables*. London, 2013.

[20] ENTSO-E. *Use of travelling waves principle in protection systems and related automations*. Brussels, 2021. URL: https://www.entsoe.eu/Documents/USE_OF_TRAVELLING_WAVES_PRINCIPLE_IN_PROTECTION_SYSTEMS_AND_RELATED_AUTOMATIONS.pdf (visited on 07/18/2016).

[21] ABB. *Technical note 2.1 – Travelling waves – Overvoltage protection*. eng. Wettingen, 2019. URL: https://search.abb.com/library/Download.aspx?DocumentID=1HC0138871&LanguageCode=en&DocumentPartId=&Action=Launch (visited on 07/22/2021).

[22] Morrison, R. *Digital circuit boards mach 1 GHz*. Hoboken, N.J, 2012.

[23] Yu, B.-X., Li, R., Su, J.-C., Zhao, L., Zhang, Y., Zheng, L., Zeng, B., Cheng, J., Gao, P.-C., Qiu, X.-D. and Xu, X.-d. *Analysis of the match problem of a capacitive voltage divider with a long measurement cable*. Measurement science technology 28.9 (2017). ISSN: 0957-0233.

[24] Ferrero, A., Petri, D., Carbone, P. and Catelani, M. *Modern measurements : fundamentals and applications*. Piscataway, New Jersey : IEEE Press ; Hoboken, NJ : John Wiley and Sons, Inc. [Online]., 2015.

[25] *12 Things to Consider When Choosing an Oscilloscope*. Tektronix, 2015 [Online]. URL: https://www.mouser.com/pdfdocs/Tektronix12_things_to_consider1.pdf.

[26] *DIAS 733 Impulse Voltage Test System: datasheet*. Available: directindustry.com > DIAS 733 > Catalogs > DIAS® 733. Basel, Switzerland: Haefely Test AG / Hipotronics INC.

[27] *PXIe, 400 MHz, 1 GS/s, 14-bit PXI Oscilloscope*. 375320g. Rev. 01. National Instruments. 2019. URL: https://www.ni.com/fi-fi/shop/hardware/products/pxi-oscilloscope.html?modelId=123641.

[28] Hällström, J. and Havunen, J. *Certificate of Calibration M-20E279: Digitizer NI PXIe-5164*. Espoo, 2020.

[29] Marston, R. *Newnes Passive and Discrete Circuits Pocket Book*. Vol. 2nd ed. ID: Accession Number: 104913. Oxford: Newnes, 2000, pp. 90–94. ISBN: 9780750641920.

[30] Havunen, J., Hällström, J., Bergman, A. and Bergman, A. *Using Deconvolution for Correction of Non-Ideal Step Response of Lightning Impulse Digitizers and Measurement Systems*. Ed. by R. Díaz. 20th International Symposium on High Voltage Engineering, ISH 2017. France: Conseil international des grands réseaux électriques (CIGRE), 2017. ISBN: 978-987-45745-6-5. DOI: 10.5281/zenodo.3568022.

APPENDIX A: CALIBRATIONS, DEC. -21

Calibration results for CS1000kV & DiAS 733

		Test voltage U_t				Front time T_1				Time to half-value T_2			
Impulse	Nominal test voltage [kV]	Reference system reading [kV]	Calibrated system reading [kV]	Error	Uncertainty	Reference system reading [µs]	Calibrated system reading [µs]	Error	Uncertainty	Reference system reading [µs]	Calibrated system reading [µs]	Error	Uncertainty
Standard front	50	51.55	50.05	-2.9 %		1.179	1.15	-2.7 %		46.40	46.82	0.9 %	
	100	103.3	100.1	-3.1 %		1.180	1.14	-3.4 %		46.38	46.80	0.9 %	
	200	206.8	200.3	-3.2 %		1.198	1.17	-2.5 %		46.74	47.16	0.9 %	
	300	309.7	300.2	-3.1 %		1.204	1.18	-2.0 %		47.16	47.58	0.9 %	
	400	398.4	385.8	-3.2 %		1.207	1.19	-1.6 %		47.65	48.03	0.8 %	
Long front	100	92.67	89.95	-2.9 %		1.526	1.53	0.1 %		47.06	47.36	0.6 %	
Short front	100	96.96	93.70	-3.4 %		0.880	0.84	-5.1 %		45.54	46.07	1.2 %	
			AVE	-3.1 %			AVE	-2.5 %			AVE	0.9 %	
			MIN	-3.4 %			MIN	-5.1 %			MIN	0.6 %	
			MAX	-2.9 %			MAX	0.1 %			MAX	1.2 %	
			DIFF	0.3 %			DIFF	2.6 %			DIFF	0.3 %	
			DIFF / SQRT(3)	0.1 %			DIFF / SQRT(3)	1.5 %			DIFF / SQRT(3)	0.2 %	

Calibration results for CS1000kV & NI
Calculating calibrated system value based on three measurements

		Test voltage U_t				Front time T_1				Time to half-value T_2			
Impulse	Nominal test voltage [kV]	Reference system reading [kV]	Calibrated system reading [kV]	Error	Uncertainty	Reference system reading [µs]	Calibrated system reading [µs]	Error	Uncertainty	Reference system reading [µs]	Calibrated system reading [µs]	Error	Uncertainty
Standard front	50	51.55	51.27	-0.5 %		1.179	1.173	-0.5 %		46.40	46.48	0.2 %	
	100	103.3	102.8	-0.5 %		1.180	1.169	-1.0 %		46.38	46.46	0.2 %	
	200	206.8	205.7	-0.6 %		1.198	1.195	-0.2 %		46.74	46.73	0.0 %	
	300	309.7	307.8	-0.6 %		1.204	1.205	0.1 %		47.16	47.21	0.1 %	
	400	398.4	396.2	-0.6 %		1.207	1.211	0.3 %		47.65	47.64	0.0 %	
Long front	100	92.67	92.15	-0.6 %		1.526	1.544	1.2 %		47.06	47.08	0.0 %	
Short front	100	96.96	96.08	-0.9 %		0.880	0.862	-2.0 %		45.54	45.76	0.5 %	
			AVE	-0.6 %			AVE	-0.3 %			AVE	0.1 %	
			MIN	-0.9 %			MIN	-2.0 %			MIN	0.0 %	
			MAX	-0.5 %			MAX	1.2 %			MAX	0.5 %	
			DIFF	0.3 %			DIFF	1.7 %			DIFF	0.4 %	
			DIFF / SQRT(3)	0.2 %			DIFF / SQRT(3)	1.0 %			DIFF / SQRT(3)	0.2 %	